AGU PUBLICATIONS

Tectonics

RESEARCH ARTICLE
10.1002/2014TC003725

Key Points:
- The anticline grew by interplay between folding and strike-slip faulting
- Analysis of calcite veins allowed constraining the timing of deformation
- The anticline developed by positive inversion

Correspondence to:
F. Storti,
fabrizio.storti@unipr.it

Citation:
Storti, F., F. Balsamo, L. Clemenzi, M. Mozafari, M. H. N. Al-Kindy, J. Solum, R. Swennen, C. Taberner, and C. Tueckmantel (2015), Complex fault-fold interactions during the growth of the Jabal Qusaybah anticline at the western tip of the Salakh Arch, Oman, *Tectonics*, *34*, 488–509, doi:10.1002/2014TC003725.

Received 29 AUG 2014
Accepted 19 FEB 2015
Accepted article online 23 FEB 2015
Published online 20 MAR 2015

Complex fault-fold interactions during the growth of the Jabal Qusaybah anticline at the western tip of the Salakh Arch, Oman

F. Storti[1], F. Balsamo[1], L. Clemenzi[1], M. Mozafari[2], M. H. N. Al-Kindy[3], J. Solum[4], R. Swennen[2], C. Taberner[4], and C. Tueckmantel[4]

[1]Natural and Experimental Tectonics Research Group, Department of Physics and Earth Sciences "Macedonio Melloni", University of Parma, Parma, Italy, [2]Department of Earth and Environmental Sciences, KU Leuven, Leuven, Belgium, [3]Petroleum Development of Oman, Muscat, Sultanate of Oman, [4]Shell Global Solutions International B. V., Rijswijk, Netherlands

Abstract The Jabal Qusaybah anticline is located at the western end of the Salakh Arch, a major salient in the foothills of the Oman Mountains. We performed a structural and petrographical-geochemical study of vein sets and fault zones associated with the development of this anticline. Our data illustrate a complex deformation pattern both in space and time, characterized by the unusual presence of widespread NE-SW left-lateral strike-slip fault zones trending oblique to the E-W fold axial strike, and of abundant and well-developed N-S fold-perpendicular extensional fault zones associated with axial bulging and dilation, well developed in the central region of the anticlinal crest. We propose a three-stage evolution for the Jabal Qusaybah anticline, starting with prefolding jointing in the foreland of the late Cretaceous Oman Mountains, and followed by development of extensional faulting in Campanian times. Positive inversion of the Qusaybah Fault, possibly in Miocene times, caused development of a layer-parallel shortening fabric and amplification the Jabal Qusaybah Anticline, in concomitance with the activity of NE-SW left-lateral strike-slip fault zones that triggered N-S, fold-perpendicular extensional faulting, particularly in the axial bump of the anticline. The final evolutionary stage was characterized by further amplification of the axial bump and related N-S extensional fracturing and by uplift and exhumation. To explain the complex noncylindrical fault-fold interactions in the study anticline, we tentatively propose that they were triggered by near foredeep-parallel tapering of the sedimentary/tectonic overburden of the Ara evaporites.

1. Introduction

Fold kinematics in shallow thrust-fold belts is driven by a number of factors, including the intimate interplay with underlying faults [e.g., *Suppe*, 1983; *Richard et al.*, 1991; *Fischer et al.*, 1992; *Bellahsen et al.*, 2006; *Tavani et al.*, 2006], the mechanical stratigraphy of the deformed multilayer [*Corbett et al.*, 1987; *Woodward and Rutherford*, 1989; *Protzman and Mitra*, 1990; *Gross*, 1995; *Couzens and Wiltschko*, 1996; *Erslev and Mayborn*, 1997; *Fischer and Jackson*, 1999; *Chester*, 2003; *Di Naccio et al.*, 2005], the fluid system structure [e.g., *Evans and Fischer*, 2012], the overburden [*Chester et al.*, 1991; *Jamison*, 1992; *Lemiszki et al.*, 1994], the tectonosedimentary inheritance [*Guiton et al.*, 2003; *Ahmadhadi et al.*, 2008; *Jahani et al.*, 2009; *Amrouch et al.*, 2010; *Beaudoin et al.*, 2012; *Sassi et al.*, 2012], and the ratio between tectonic uplift and syntectonic sedimentation rates [e.g., *Storti and Salvini*, 1996; *Barrier et al.*, 2002]. The synergic use of stratigraphical, structural, and petrographic/geochemical information allows major improvements to be made in the study of fault-related folds [*Swennen et al.*, 2003; *Roure et al.*, 2005; *Barbier et al.*, 2012a, 2012b; *Beaudoin et al.*, 2013] and foreland belts [*Callot et al.*, 2010], particularly in foreland and hydrocarbon prone settings.

Fold development in curved deformation front segments may imply further complexities because the formation of salients and recesses is triggered by local variations of the geological conditions at the wedge toe [e.g., *Macedo and Marshak*, 1999; *Muñoz et al.*, 2013], including the presence of inherited preorogenic fault zones and of evaporites [e.g., *Anastasio and Holl*, 2001; *Jahani et al.*, 2009]. The arcuate shape of salients and recesses is typically accompanied by noncylindrical deformations and partitioning between dip-slip and strike-slip faulting [e.g., *Marshak*, 1988]. In such a geological framework, the expected fold-related deformation pattern may significantly deviate from the classical longitudinal and transversal distribution of deformation structures [e.g., *Stearns*, 1968; *Storti and Salvini*, 1996] described in cylindrical thrust-related folds

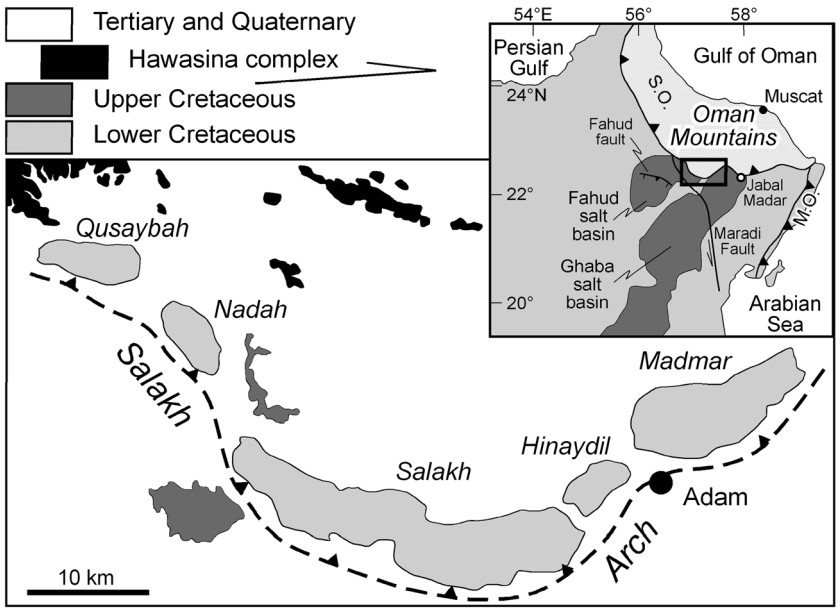

Figure 1. Geological sketch map of the Salakh Arch, northern Oman. The arrow in the upper left of the figure and the associated rightward displacement of the black rectangle indicate detachment and overthrusting of the Hawasina complex. The inset shows the location of the arch at the southern deformation front of the Oman Mountains [*Al-Kindi*, 2006; *Filbrandt et al*., 2006]. M.O. means Masirah Ophiolite; S.O. means Semail Ophiolite.

[e.g., *Hancock*, 1985; *Cooper*, 1992; *Tavani et al*., 2006, 2008]. Given the importance that fault-fold growth in thrust-fold belts and accretionary prisms has for both economical and seismic hazard mitigation purposes, descriptions of the kinematic evolution of anticlines developed within thrust salients and recesses can provide effective analogs to support predictions of deformation patterns and related fluid flow in comparable subsurface settings.

In this paper, we describe the type and orientation of faulting- and folding-related deformation structures exposed in the Jabal Qusaybah anticline, which is located at the western inflection point of the Salakh Arch, in northern Oman. Petrographical and isotopical characterization of vein networks provide additional constraints to the relative chronology of folding- and faulting-related deformation structures established in the field. By combining field and laboratory information, an evolutionary pathway is proposed for the Jabal Qusaybah anticline where positive fault inversion, strike slip, and extensional faulting, as well as fold amplification above a basal evaporitic décollement layer, coevally interact.

1.1. Geological Setting

The Jabal Qusaybah anticline is located at the western termination of the Salakh Arch, the large salient that characterizes the southern deformation front of the Northern Oman Mountains (Figure 1). The stratigraphic succession in the footwall of the ophiolitic nappes includes Precambrian carbonates and siliciclastic rocks, a Paleozoic section dominated by siliciclastic rocks, and Mesozoic to Cenozoic carbonates with subordinate interlayered siliciclastic formations. The presence of the Early Cambrian Ara evaporites (Fahud and Ghaba salt basins; Figure 1) supports the inference that the basal thrust of the Salakh Arch is localized within these evaporites [*Hanna*, 1990; *Al-Kindi*, 2006; *Filbrandt et al*., 2006]. The Cretaceous stratigraphic pile starts with the platform carbonates of the Kahmah Group, separated by an unconformity from the shales and sandstones of the Nahr Umr Formation. Another major unconformity separates the latter from the carbonate Natih Formation whose upper part is in turn eroded and unconformably overlain by the shales and sandstones of the Aruma Group [e.g., *Homewood et al*., 2008] (Figure 2).

Jabal Qusaybah exposes an about 8 km long, 3 km wide anticline (Figure 3) where the Cretaceous Natih Formation and, in particular, the lithostratigraphic members A (Late Cenomanian-Early Turonian), B (Middle–Late Cenomanian) and C (Middle Cenomanian) crop out. The former mainly consists of platform carbonates and overlies the intrashelf basinal carbonates of the B member. A more competent horizon

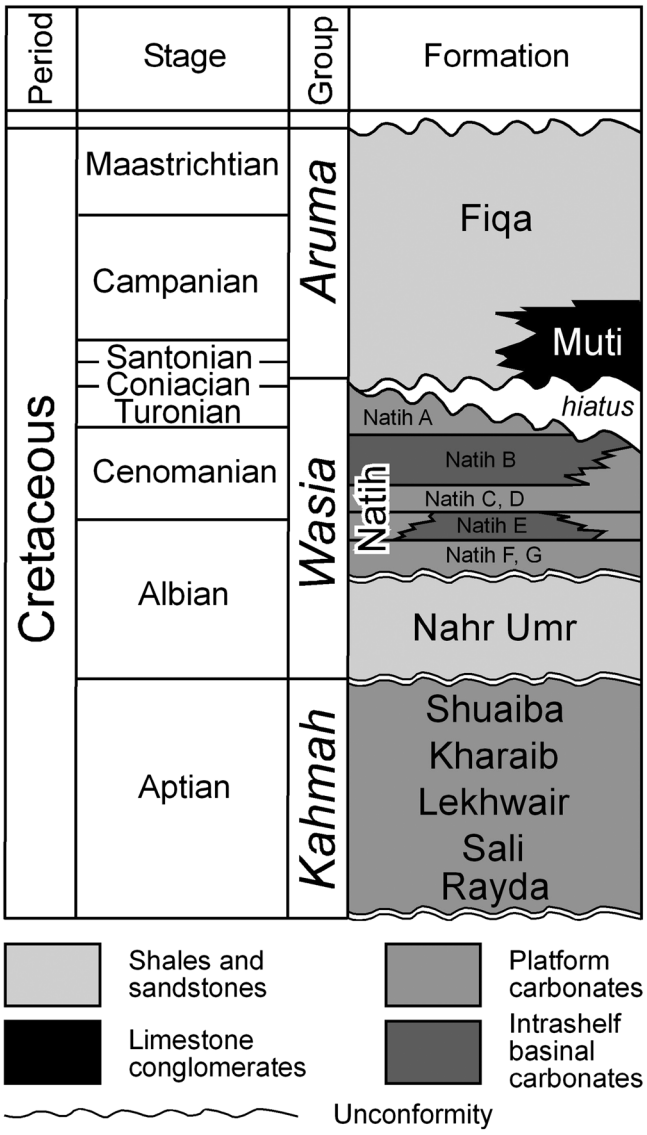

Figure 2. Stratigraphic column of the Cretaceous rocks exposed in the Oman Mountains [*Filbrandt et al.*, 2006; *Homewood et al.*, 2008].

occurs within Natih B and provides a useful key layer for stratigraphic correlations. Natih C mainly consists of platform carbonates and its top is characterized by a yellowish horizon of coarse-grained rudist debris forming a tidal sandwave [e.g., *Hanna and Smewing*, 1996; *Homewood et al.*, 2008] (Figures 2 and 4).

The hinge line of the Jabal Qusaybah anticline strikes almost E-W and the exposed cross-sectional fold shape is open and slightly asymmetrical to the north. In the central sector of the fold a peculiar symmetrical bulge occurs (Figure 5). A characteristic structural feature of this anticline is the presence of linked NE-SW left-lateral strike-slip and N-S extensional fault zones. Left-lateral fault zones have an oblique trend with respect to the fold strike and N-S extensional fault zones are confined within strike-slip-bounded compartments that characterize the central part of the fold. Moreover, N-S extensional fault zones also occur at the southwestern tip of the left-lateral strike-slip fault zones where they terminate within the anticline. As a whole, the fault network creates a left-lateral transtensional horsetail array localized in the longitudinal axial bulge of the anticline (Figure 3). A segmented N-S right-lateral strike-slip fault zone occurs to the west and is localized along the hinge between the flat-lying crestal region, and the western limb of the central axial bump (site G in Figure 3).

The two-dimensional seismic profile AR40984 [*Al-Lazki et al.*, 2002] was reinterpreted to illustrate the subsurface architecture of the Jabal Qusaybah anticline. The profile was acquired to the west of the exposed anticline along a NE-SW trajectory (Figure 6a), so it describes the periclinal fold geometry. Formation tops of Natih (Cenomanian-Turonian), Akhdar (top Triassic), Gharif (Late Permian), and Huqf (Early Cambrian) in the undeformed foreland, and the base of the allochthonous Hawasina Complex to the north, are from *Al-Lazki et al.* [2002] and *Al-Kindi* [2006]. The most evident tectonic feature is an antiformal structure that occurs in the northeastern half of the profile. The area of increased noise due to seismic velocity pull-up that vertically projects below the anticline, does not allow detecting with confidence the geometry of the interpreted reference layers in this part of the seismic profile. For this reason, the possible occurrence of an inherited Precambrian extensional fault zone below the Ara evaporites cannot be neither excluded nor supported. A northward dipping extensional growth fault is preserved in the footwall of the fold. The seismic data indicate that this fault was active during the deposition of the Campanian lower Fiqa Formation and is sealed by gently southward dipping and thinning foredeep sediments (Figure 6a). The gentle anticlinal folding well imaged to the SW of the anticline suggests fault-related mobilization of the Ara evaporites [*Al-Lazki et al.*, 2002; *Al-Kindi*, 2006]. A depth-converted interpretation of the anticline is proposed,

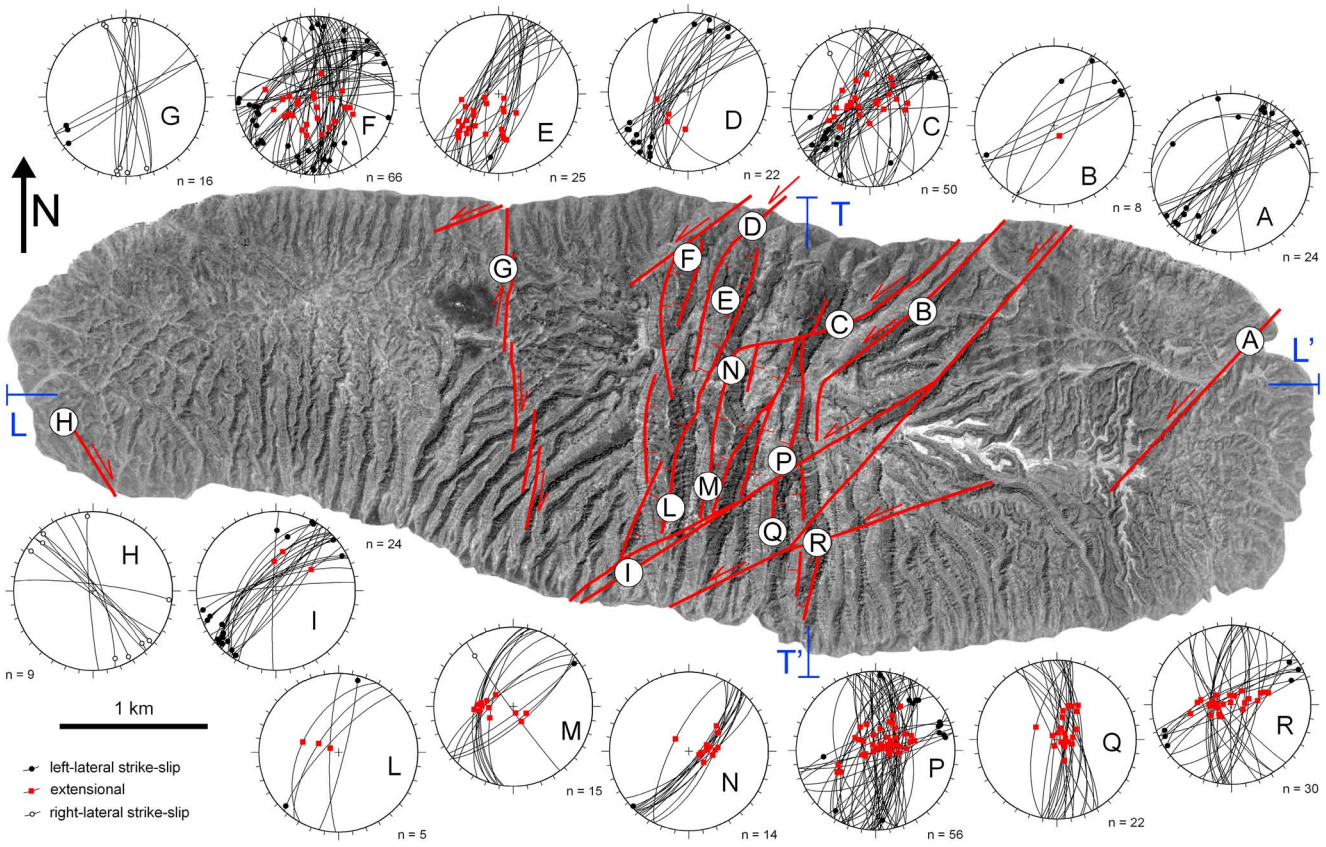

Figure 3. Network of major fault zones mapped in Jabal Qusaybah (image from Google Earth) and stereographic projections of fault data collected in field localities A to R. The tip points of cross sections L-L′ and T-T′ (Figure 5) are indicated. In this and the following figures, stereographic projections of planar surfaces are on the Wulff equal angle net, lower hemisphere.

constrained by cross-section balancing (Figure 6b). It shows a pop-up structure produced by positive inversion of a NE dipping listric extensional fault zone and a SW dipping antithetic one. Backthrusting along the latter during fold tightening caused crosscutting and reverse displacement of the former master fault. Eventually, a NE dipping reverse fault zone cutting through the backthrust developed in the footwall. Restoration of the interpreted tectonosedimentary pattern provides the geometry of the Qusaybah extensional fault zone in Campanian times (Figure 6c).

2. Data Presentation

Deformation structures exposed in the Jabal Qusaybah anticline consist mostly of calcite veins, extensional and strike-slip fault zones, and stylolites. The deformation pattern is characterized by a high complexity produced by multiple fracturing events along the same trends and nonsystematic overprinting relations. To address such a complexity, a fully integrated approach involving structural, petrographical, and geochemical analyses, was used. To facilitate data presentation, we first describe the petrography and geochemistry of cements and then illustrate the deformation pattern. In this study, representative samples from veins and fault core infills are described for relative chronology purposes (Figure 7), whereas the complete data set is presented in a forthcoming paper.

2.1. Analytical Methods for Vein Characterization

To evaluate the iron content in dolomite and calcite, polished rock slabs and thin sections were stained using Alizarine red S and potassium ferricyanide [*Dickson*, 1966]. Cold cathodoluminescence microscopy was carried out using a modified Technosyn cathodoluminescence device model 8200, Mark II, operating at 10–16 kV gun potential, 200–400 μA gun current, 0.05 torr vacuum, and 5 mm beam width. Samples for stable oxygen

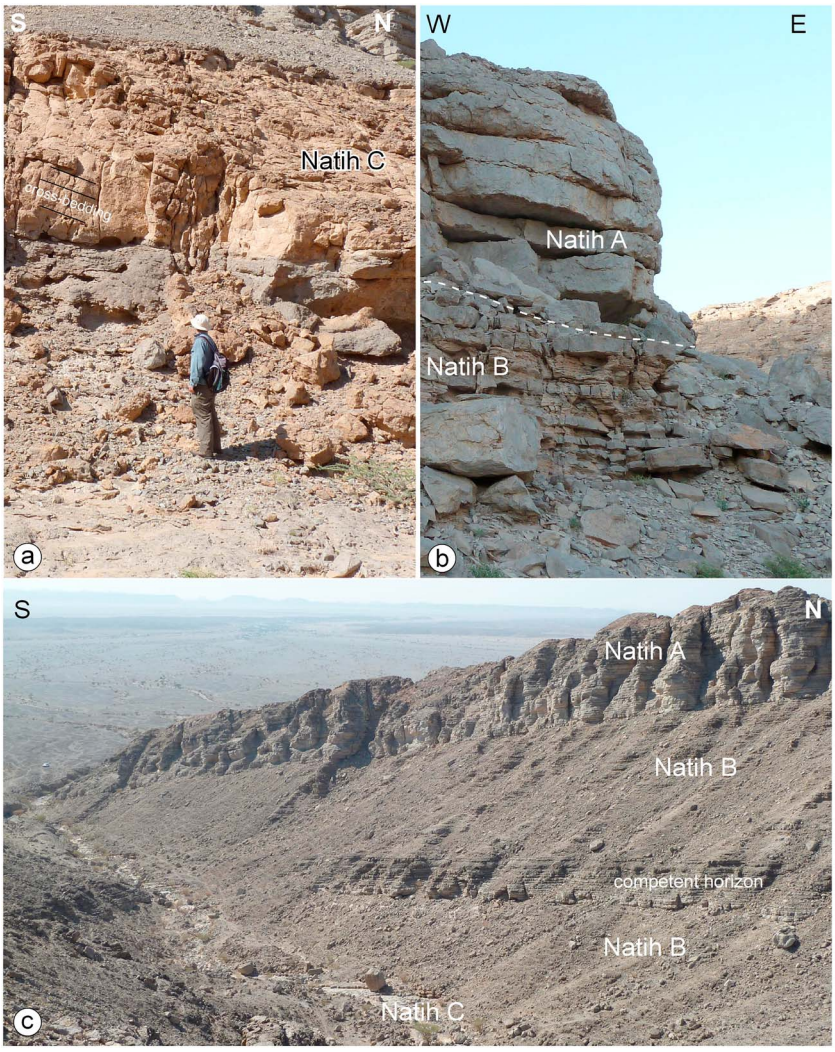

Figure 4. (a) Yellowish coarse bioclastic grainstone with large cross beds at the top of Natih C; field locality C in Figure 3. (b) Detail of the stratigraphic contact between Natih A and B lithostratigraphic members; field locality P in Figure 3. (c) Panoramic view of the southern limb of the Jabal Qusaybah anticline (photo from locality P in Figure 3, looking southward) showing the appearance of the exposed stratigraphic succession from Natih C to A.

and carbon isotope analysis were collected employing a dental drill and Merkantec micromilling device. They were analyzed at the Friedrich-Alexander-Universität (Erlangen-Nuremberg, Germany) and the Vrije University Amsterdam (the Netherlands) using a ThermoFinnigan Five Plus and Finnigan DeltaPlus isotope ratio mass spectrometer, respectively. All values are reported in per mil relative to Vienna Pee Dee Belemnite (VPDB).

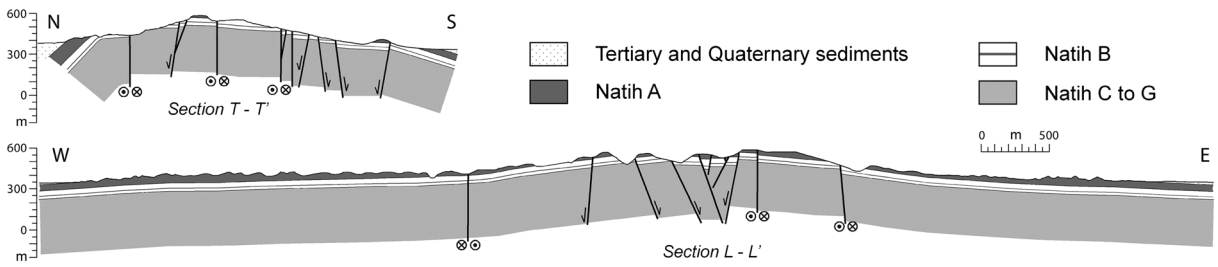

Figure 5. Transversal (T-T') and longitudinal (L-L') geological cross sections illustrating the main geometric features and fault zone distribution in the Jabal Qusaybah anticline. See Figure 3 for location.

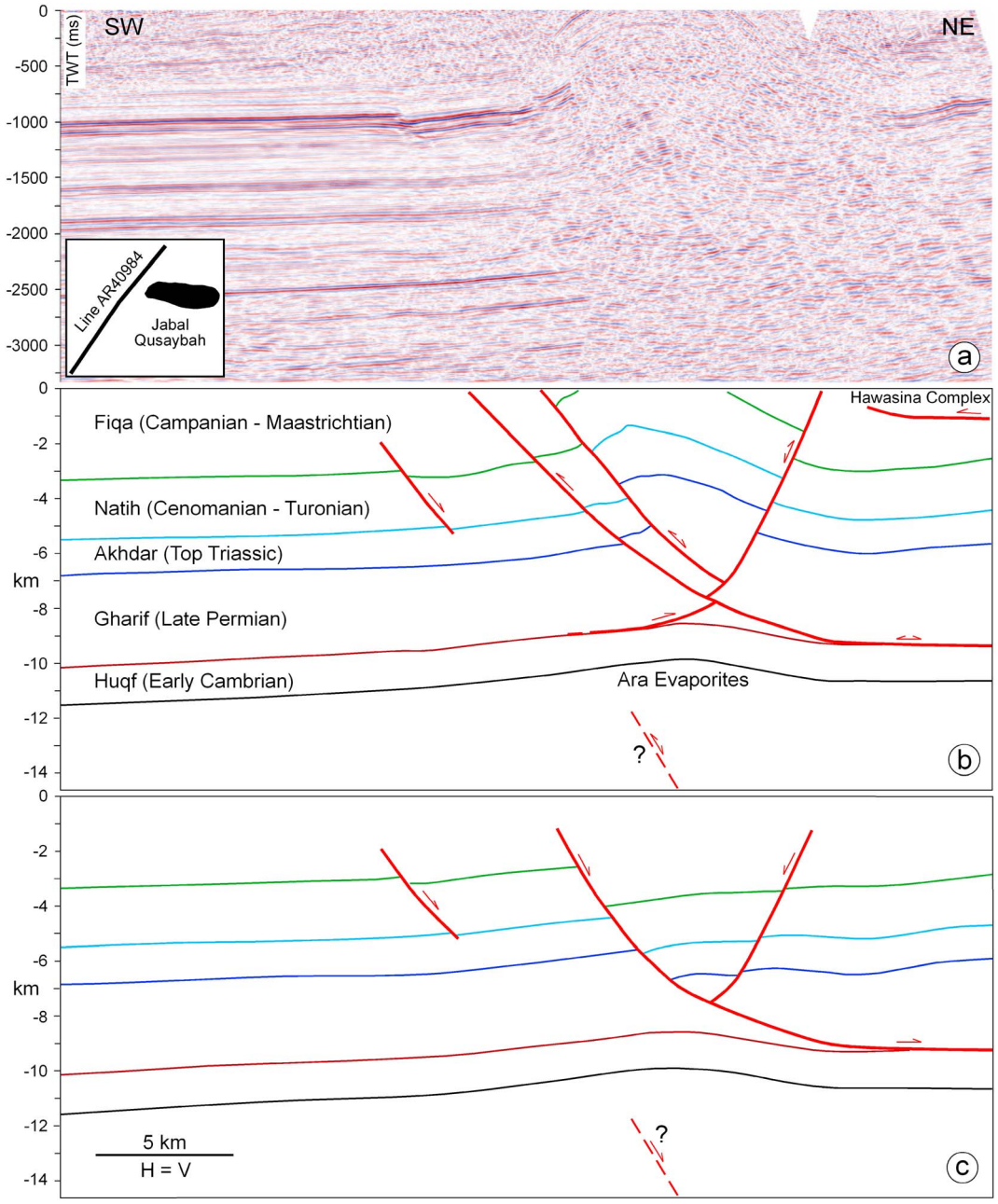

Figure 6. (a) Line AR40984 and (b) its proposed interpretation, illuminating the cross-sectional geometry in the western pericline of the Jabal Qusaybah anticline. (c) The depth-converted and restored version of the proposed interpretation is provided. See text for details.

Several cement generations were identified, which can be best described by subdividing them into three main groups, each representing unique precipitation conditions attributed to fluid circulation linked to the three major stages of tectonic deformation.

2.2. Petrography and Geochemistry of Group 1 Veins

Group 1 veins consist of nonferroan, cloudy white calcite crystals with a thickness not exceeding 1–2 cm. They are intensely affected by tightly spaced mechanical twinning (Types II and III of *Burkhard* [1993]). The cathodoluminescence (CL) pattern is characterized by nonluminescence (Figures 7c and 7d). Group 1 veins and E-W tectonic stylolites mutually crosscut. The $\delta^{18}O$ and $\delta^{13}C$ composition of Group 1 veins

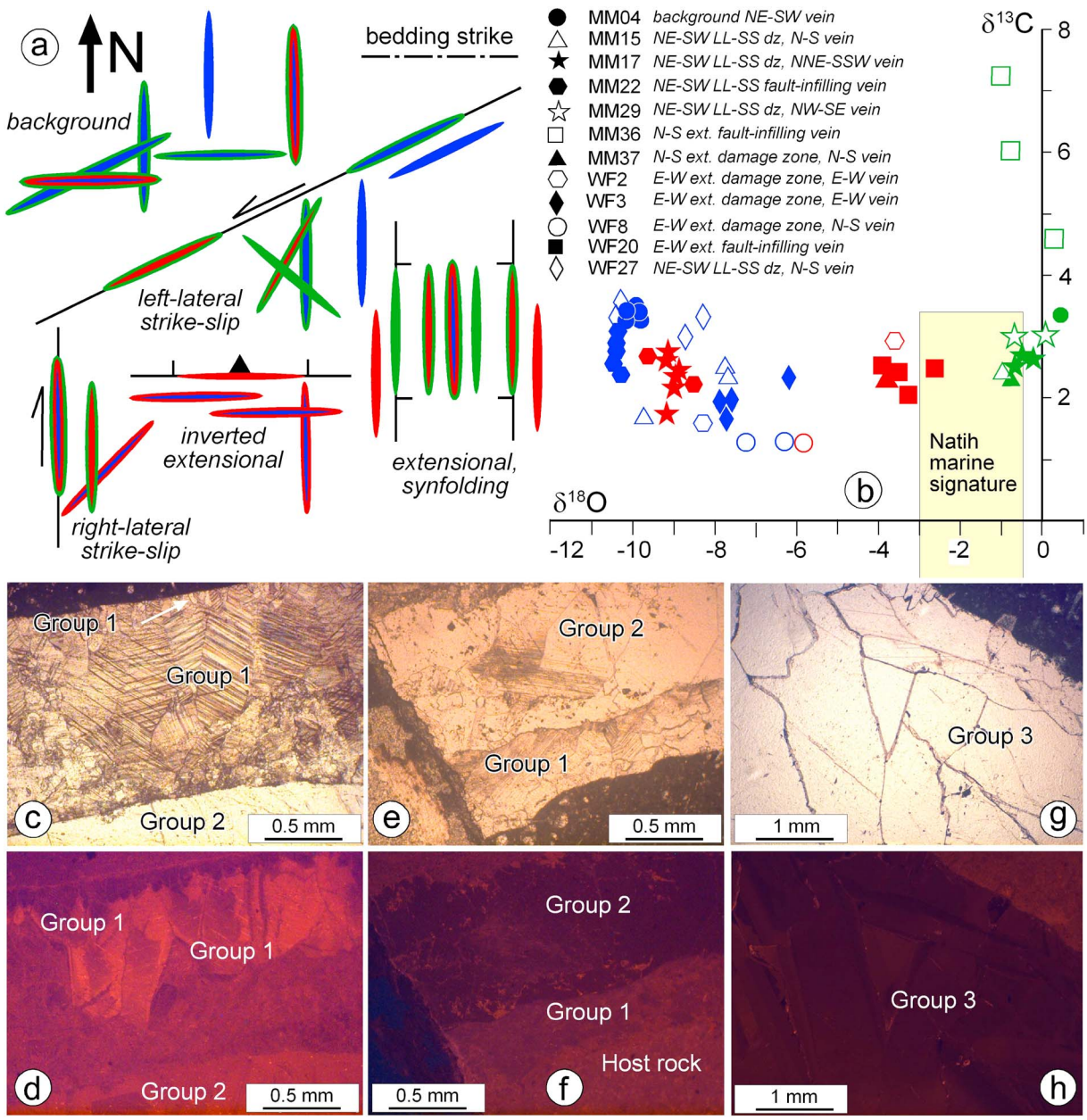

Figure 7. Petrographical and geochemical characterization of calcite vein sets. (a) Conceptual sketch map of fault-vein arrays in Jabal Qusaybah: veins are oriented with respect to the geographic north, and their colors indicate the relative chronology of calcite precipitation (multiple colors indicate vein reopening): dark blue indicates Group 1 cements, red indicates Group 2 cements, and green indicates Group 3 cements. (b) Cross plot $\delta^{13}C$ versus $\delta^{18}O$ of the analyzed veins and fault core infillings; same color code as in Figure 7a; LL-SS dz means left-lateral strike-slip damage zone, ext. means extensional. (c) Sample WF03: photomicrograph in plane polarized light of Group 1 calcite generation, reopened by Fe-rich Group 2 calcite. Note the deformational twins in Group 1 crystals. (d) Cathodoluminescence image of the same view as shown in Figure 7c. Note the two different cathodoluminescence (CL) patterns in Group 1 calcites (1a and 1b, respectively). The non-CL crystals predate the crystals with brown CL possessing a slight zonation pattern. (e) Sample WF02: photomicrograph in plane polarized light of Group 1b calcite reopened by Fe-rich Group 2 calcite. Note the deformational twins in Group 1 crystals. A fragment of Group 1 vein is embedded in Group 2 blocky crystals (untwinned). (f) Cathodoluminescence image of the same view as shown in Figure 7e, showing brown CL pattern in twinned Goup 1 calcite and dull brown in Group 2 calcite. (g) Photomicrograph in plane polarized light of Group 3 calcite crystals. (h) Cathodoluminescence image of the same view as shown in Figure 7g, illustrating brown CL pattern with sector zonation.

varies between −10.3 and −8.1‰ VPDB and between +3.0 to +3.5‰ VPDB, respectively (Figure 7b). For comparison purposes, the stable isotope signatures of the Natih marine carbonate host rocks measured in Jabal Qusaybah range for $\delta^{18}O$ between −3.0 and −0.5‰ VPDB and for $\delta^{13}C$ between −1.0 and +3.5‰ VPDB [*Immenhauser et al.*, 2000].

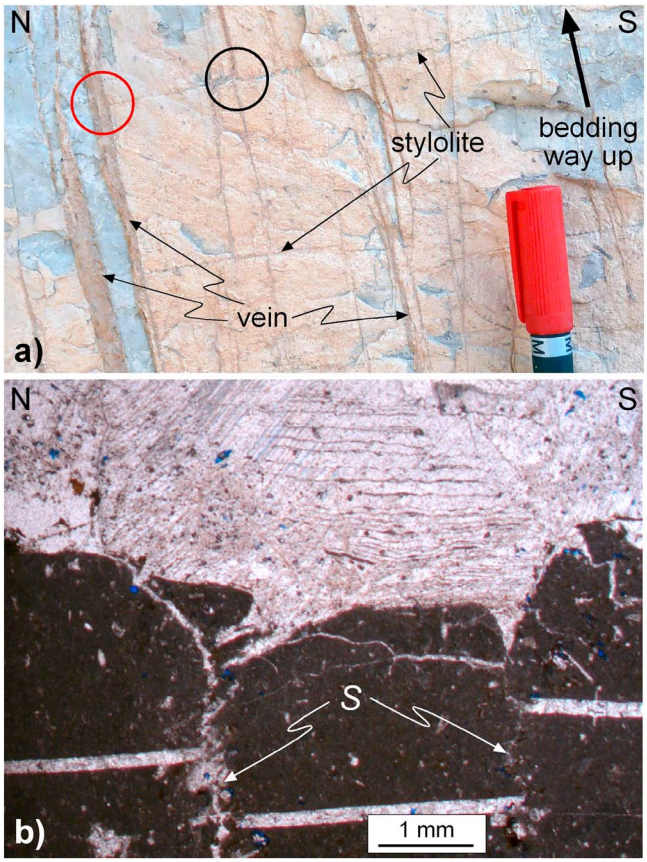

Figure 8. (a) Cross-sectional view of a thick Natih A limestone bed showing mutually overprinting relations between bedding parallel stylolites and veins (field locality E in Figure 3, arrow indicates the stratigraphic up direction). A stylolite overprints a vein in the area indicated by the black circle and is overprinted by another vein, striking parallel to the previous one, in the area indicated by the red circle. (b) Microphotograph from a bedding-parallel thin section (field locality E in Figure 3) showing E-W near-vertical stylolites (S) overprinting a N-S near-vertical thin calcite vein. They are in turn overprinted by a N-S near-vertical large calcite vein with evidence of crack-seal opening (plane polarized light).

2.3. Petrography and Geochemistry of Group 2 Veins

Group 2 veins span from millimeter-scale to several decimeter thick fractures and fault infills and contain nonferroan, slightly ferroan to ferroan randomly oriented blocky calcites. The early crystals are characterized by a milky white to pale yellow color and intense deformational twins (Types II and III of *Burkhard* [1993]) with undulose extinction indicating tectonic deformation. Conversely, late crystals in both fault core infills and veins have black, grey, or translucent white colors, depending on amount of crystal impurities, with pervasive brown alterations in hand specimen. In thin section they have less or no twinning (Figure 7e). The CL pattern of early crystals in Group 2 calcites is brown and dull exhibiting slight zonation luminescence while later crystals display relatively homogenous brown in nonaltered samples. However, also, blotchy outlines occur which are interpreted to correspond with recrystallized portions (Figure 7f). The δ^{18}O signatures of this group of calcite display a wide range varying between −10.4 and −2.6‰ VPDB. This large spread likely reflects the existence of several subgenerations of calcite that, for the purposes of this work, are grouped together. In contrast their δ^{13}C composition displays a relatively narrow range of +1.3 to +3.0‰ VPDB (Figure 7b).

2.4. Petrography and Geochemistry of Group 3 Veins

Group 3 vein size spans from millimeter-scale microfractures to meter-scale fault infills. They possess a variable low to intermediate Fe content, and their typical color is white to translucent white, with grey growth zones characterized by minor yellow to brown alterations if compared to Group 2 calcites. The crystals are commonly elongate with axial length perpendicular to the fracture walls, exhibiting brown CL color with sector zonation (Figures 7g and 7h). The size of crystals reaches up to about 30 cm in fault infillings characterized by bladed to scalenohedral crystals. The δ^{18}O compositions demonstrate relatively less depleted values ranging between −1 and +0.1‰ VPDB. The δ^{13}C composition varies between +3.0 and +8.0‰ VPDB (Figure 7b).

2.5. Background Deformation

Bedding-parallel stylolites are quite common, particularly in Natih A and C members. They typically are overprinted and overprint a first generation of near-vertical, white to brown NNE-SSW and E-W trending Group 1 veins (Figure 8a). Most Group 1 veins strike either parallel or perpendicular to the bedding direction, regardless of their orientation and location within the anticline (Figure 9). In the poorly layered Natih C carbonates, NE-SW striking Group 1 veins also developed as conjugate shears of the NNE-SSW set (Figures 9c and 9d). In many cases, in the Natih C the latter vein population shows evidence of

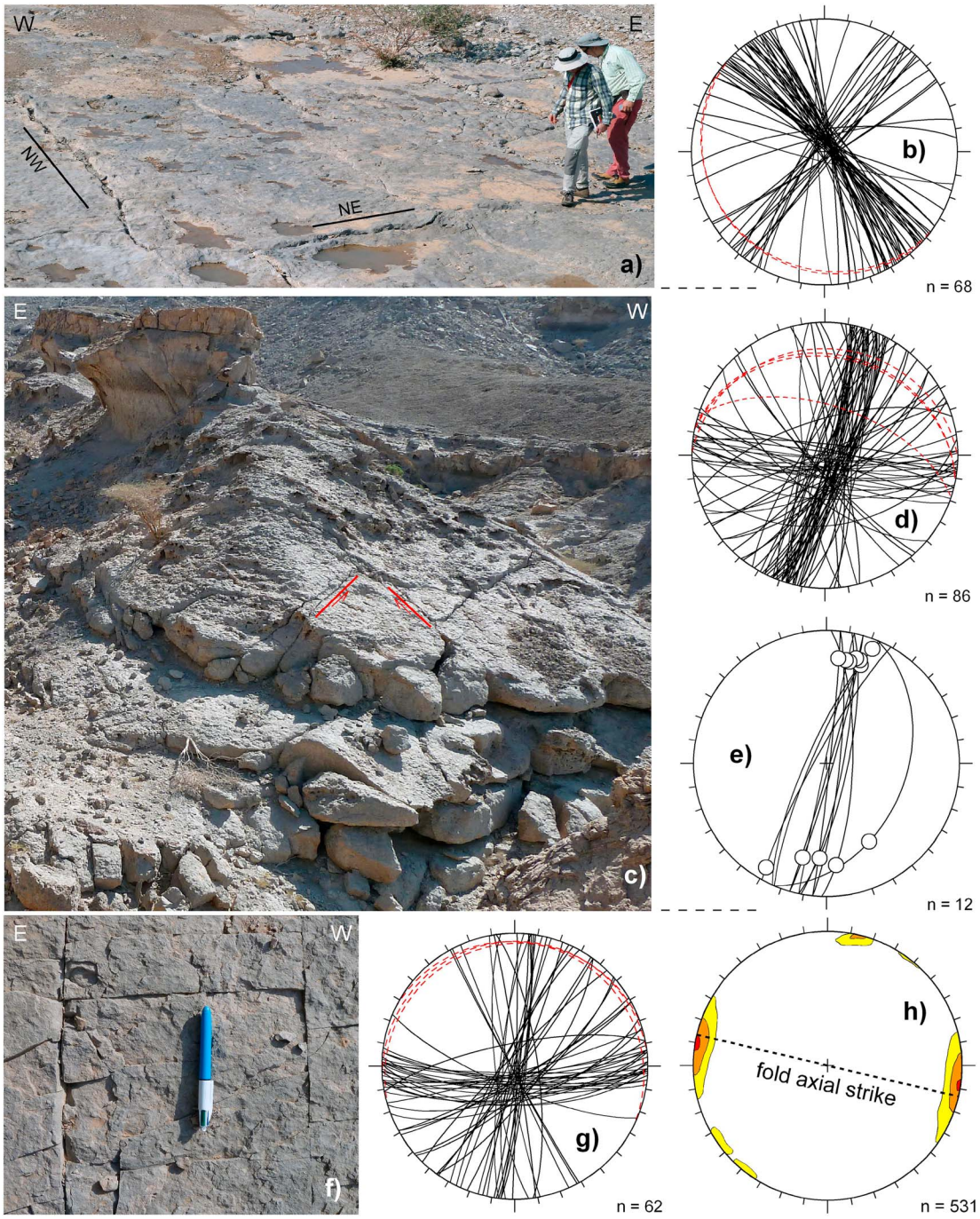

Figure 9. (a) Pavement view of NW-SE and NE-SW calcite veins and their abutting relations; Natih A, field locality H in Figure 3. (b) Stereographic projection of vein data collected in the field locality shown in Figure 9a. (c) Panoramic view, looking southward, of Natih C exposed in the forelimb of the Jabal Qusaybah anticline to show the occurrence of different vein sets (field locality E in Figure 3). (d) Stereographic projection of vein data collected in the field locality shown in Figure 9c. (e) Stereographic projection of NNE-SSW striking veins reactivated as small-scale right-lateral strike-slip faults (data collected in the same field locality as Figure 9d). (f) Plane view of a Natih B bed affected by two mutually perpendicular vein sets (field locality G in Figure 3). (g) Stereographic projection of vein data collected in the field locality shown in Figure 9f. (h) Contoured poles to vein data collected at several field localities, far from fault zones. In this and the following figures, pole contours are made on the Schmidt equal area net, lower hemisphere; when not specified, contouring is at 5% intervals. Small circles indicate slip lineations.

reactivation as small-scale right-lateral strike-slip faults (Figure 9e). Multiple reopening events of Group 1, by Group 2 veins are very common, which also occur as newly formed deformation structures. Group 3 cements precipitated along reopened Group 1 and/or Group 2 veins, and in newly formed fractures (Figure 7a).

Analysis of the entire background vein data set indicates that many of them strike NNE-SSW, with an additional set striking almost E-W, i.e., perpendicular and parallel to the fold axial strike, respectively (Figure 9h). Abutting relations indicate that in many cases veins striking parallel to bedding are confined in-between veins striking in the dip direction of beds (Figure 9f). This is particularly true for Group 1 veins, while the opposite relative chronology also occurs when Groups 2 and 3 veins are considered. Tectonic stylolites trending parallel to the fold axial strike exist at some places but are not widespread at the outcrop scale. In most cases they cut the NNE-SSW Group 1 veins and are in turn overprinted by younger veins striking parallel to the older ones and characterized by evidence of multiple opening events (Figure 8b).

2.6. Inverted E-W Extensional Fault Zones

Evidence for positive inversion of preexisting E-W extensional fault zones was found at some field localities, including locality G (Figure 3), where bedding pattern and structural data support the initial occurrence of a complex, strongly segmented northward dipping extensional fault zone affected by subsequent reverse motion (Figures 10a–10d). Two faults are exposed at the base of the cliff, and extensional kinematics is indicated in both of them by (i) subvertical, fault-related Group 1 veins striking parallel to, or at low angle from the fault plane (Figure 10c) and (ii) a preserved extensional stratigraphic throw of 4.38 and 4.26 m, respectively. A subsequent reversal of fault motion is supported by (a) subhorizontal fault-related Group 2 veins, striking parallel to the slip surface and crosscutting the subvertical veins (Figure 10c), (b) subvertical fault-parallel tectonic stylolites (Figure 10c) and (c) calcite slickenfibers on slip surfaces in the whole outcrop, indicating the occurrence of both extensional and contractional kinematics, the latter systematically being the younger motion (Figure 10d).

At a smaller scale, positive inversion of fault zones exposed at field locality C is indicated by calcite shear vein geometries on slickensides (Figures 10e and 10f). In both cases, the stratigraphic throw is still extensional. In a fault zone to the north of locality C, the former extensional kinematics is indicated by abundant fault-parallel Group 1 veins in the damage zone, while kinematic indicators on slickensides support reverse slip (Figure 10g). In the last two fault zones, positive inversion is also indicated by the presence of a gentle anticline in the hanging wall of the fault (Figures 10f and 10g). Clear evidence of positive inversion was found at field locality E, in a ENE-WSW to E-W trending fault zone characterized by a master slip surface and subsidiary faults in the footwall damage zone. Indeed, most of these faults still preserve extensional kinematics which is associated with fault-parallel, steeply dipping Group 1 veins, commonly reopened and infilled by Group 2 cements (Figures 11a–11c). However, the thick Group 2 vein infilling the ENE-WSW master slip surface shows slickenfibers indicating reverse shear. This is supported by microstructural evidence in thin section, showing tectonic stylolites that offset the former master slip surface and overprint the thick calcite vein infilling the master slip surface (Figure 11d). The orientation of stylolites is compatible with a late stage reverse motion. N-S trending Group 1 veins, reopened as Group 2, occur mainly in the hanging wall of this fault zone, predating the E-W ones (Figure 11e). At the northern boundary of this fault zone, an ENE-WSW slip surface preserves near-horizontal slickolites indicating left-lateral strike-slip shear, overprinted by steeply dipping calcite slickenfibers indicating extensional kinematics (Figure 11f).

2.7. Fault Damage Zones

Strike-slip fault damage zones contain abundant veins that are frequently arranged in two sets striking parallel (set 1) and at about 45° from the master slip surfaces (set 2), respectively (Figure 12). In many cases, Group 1 vein cement is reopened and infilled by Group 2 and/or Group 3 calcite (Figure 7a). At field locality G, centimeter-thick calcite veins adjacent to the master slip surface are tightly folded by fault drag (Figure 12b). In the same outcrop, the western wall of the right-lateral strike-slip fault zone exposes the Natih B member, which is characterized by abundant, closely spaced stylolites striking mainly NW-SE (Figure 12c). Intersections between different vein sets observed in the damage zone of a NE-SW left-lateral strike-slip fault zone at field locality D show that Group 2 NNE-SSW and NE-SW striking veins mutually overprint (Figure 13), indicating sinistral shearing and fault-parallel dilation cyclical episodes. A NE-SW left-lateral strike-slip fault zone exposed at field locality A provides relations among different calcite vein generations far from the intensely deformed central axial bulge (Figure 14). The oldest calcite veins strike about N-S, at about 60° counter clockwise from the master slip surface (set 1 in Figure 14c). They show two opening events, infilled by Group 1 and Group 3 cements, respectively. A NNE-SSW striking splay fault zone shows the same angular relations with vein set 1 (Figures 14d and 14e). Vein set 1 is overprinted by

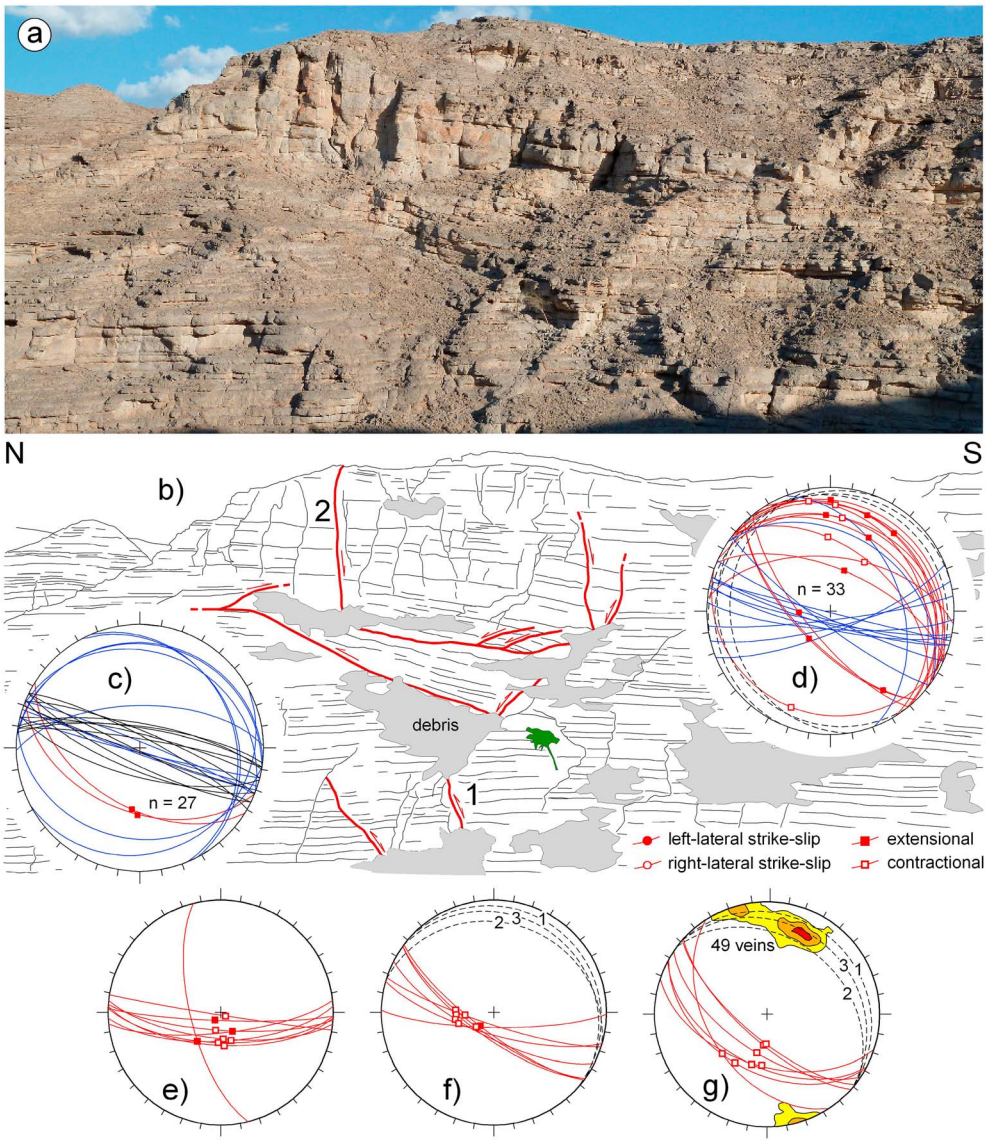

Figure 10. (a) Panoramic view of the eastern wadi wall at field locality G. Natih A limestone is exposed, showing a bedding and fault pattern that supports positive inversion of a preexisting E-W extensional fault zone. (b) Line drawing of the same image. (c) Stereographic projection of structural data collected on the two faults exposed in the lower part of the outcrop: faults are in red, veins in blue, and tectonic stylolites in black. (d) Stereographic projection of structural data collected in upper part of the outcrop: broken circles indicate the attitude of bedding. (e) Stereographic projection of fault data collected westward of field locality C. (f) Stereographic projection of fault data collected at field locality C. (g) Stereographic projection of fault and bedding data (great circles), and contoured poles to veins collected northward of field locality C. In Figures 10f and 10g, 1 refers to the attitude of bedding in the footwall of the inverted fault zone, 2 refers to bedding in the hanging wall close to the fault zone itself, and 3 refers to the average attitude of bedding outside the slightly folded area. In both cases, bedding forms a gentle anticline within the northward dipping forelimb of the host fold.

vein set 2 that trends NNE-SSW, at about 30° counterclockwise from the master slip surface (Figure 14f). Also, in this case, veins show two opening events, infilled by group 2 and group 3 cements, respectively. Finally, vein set 3 cuts across the previous deformation structures; it has Group 3 cement and trends about NW-SE, near parallel to the bedding strike (Figure 14g). Vein sets 1 and 2 are only observed in the damage zone of the fault, while vein set 3 is broadly distributed.

Extensional fault zones, apart from E-W ones affected by positive inversion, trend mostly N-S to NNE-SSW (Figure 3). Many of them dip about 60° but near-vertical fault zones showing extensional downthrows also occur (e.g., localities C, P, and Q in Figure 3). In some cases, extension-related deformation structures are

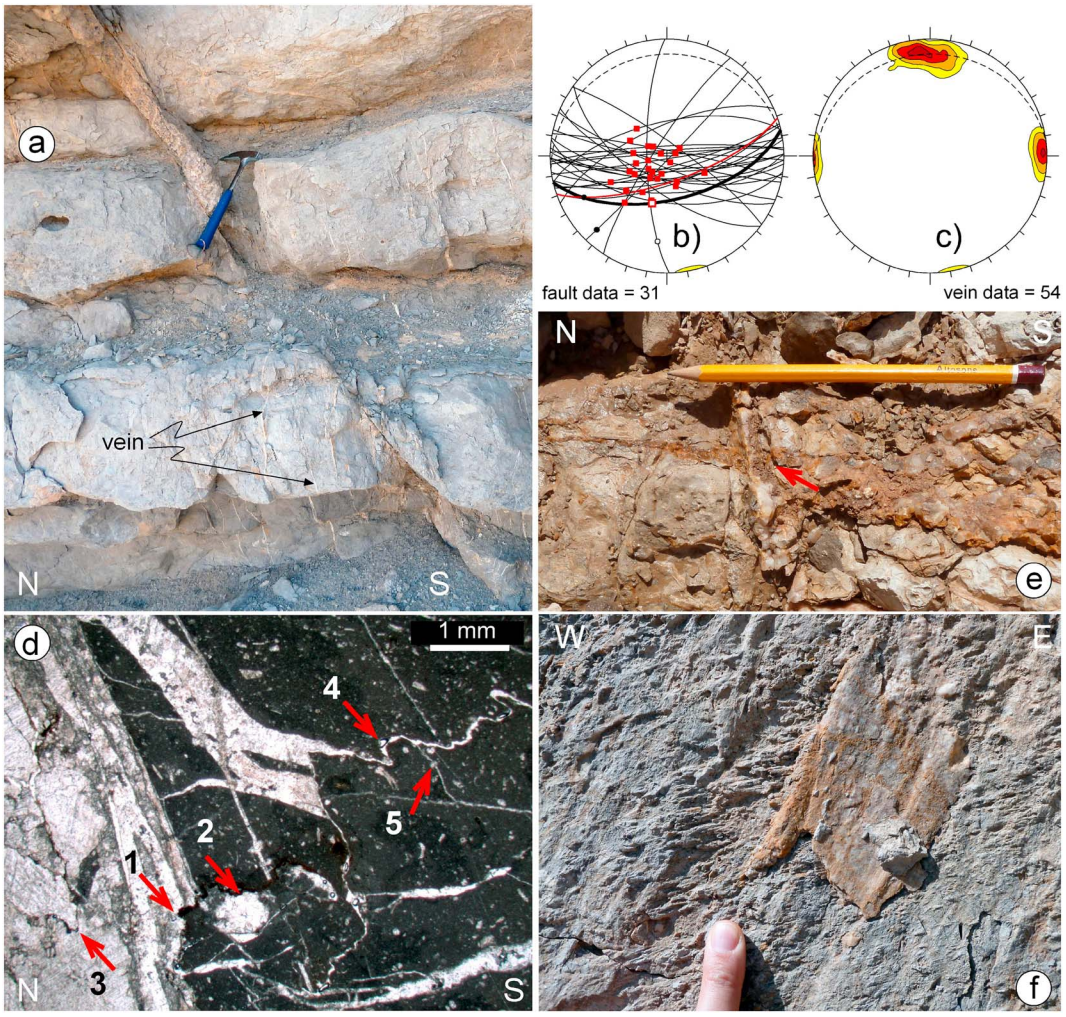

Figure 11. Example of positive inversion of an E-W extensional fault zone at field locality E. (a) Cross-sectional view of a segment of the fault zone showing abundant calcite veins both in the hanging wall and in the footwall, and the presence of a thick vein infilling the dilated master slip surface (at location of hammer). (b) Stereographic projection of fault data collected at field site a; the thicker great circle provides the orientation of the inverted master slip surface. (c) Stereographic projection showing contoured poles to veins. (d) Photomicrograph showing a detail of the thick vein infilling the dilated master slip surface and the host rock in the hanging wall. Multiple events of calcite crystallization are evident in the vein, with larger twinned crystals occurring in the central sector. The master slip surface is offset by a stylolite that affects also the host rock (arrows 1 and 2). Other dissolution surfaces are evident within both the large vein (arrow 3) and the host rock (arrow 4). In both cases, smaller calcite veins coeval with stylolites formed at some stylolitic teeths (arrows 1 and 5). The geometric relations between the master slip surface and the stylolites and related veins indicate a reverse motion overprinting the thick calcite infill. (e) Plane view of an E-W calcite vein cross cutting a N-S one. The red arrow indicates the intersection point. (f) Detail of an E-W master slip surface showing near-horizontal slickolites indicating left-lateral strike-slip motion, overprinted by calcite shear fibers developed during subsequent extensional motion.

overprinted by right-lateral strike-slip ones (Figures 15a and 15b), while in other cases they are overprinted by left-lateral strike-slip motions, particularly when the former extensional fault zones trend NNE-SSW and are located in the proximity with the NE-SW left-lateral strike-slip master fault zones (Figure 15c). In few cases, such as locality E in Figure 3, damage zones preserve the evidence of previous right-lateral strike-slip activity indicated by near-vertical stylolites making an acute angle with the strike of the extensional master slip surface (Figure 16). In approximately N-S extensional fault damage zones, near-vertical thick Group 2 veins striking parallel to the master slip surfaces are very abundant and show clear evidence of multiple calcite infilling events, the last ones characterized by Group 3 cements (Figures 15d and 15e). At field locality P, bedding parallel Group 2 veins are widespread in the footwall of a master extensional fault zone. They include decimeter-thick wedge-shaped veins that taper away from the fault core in a few meters (Figure 15f).

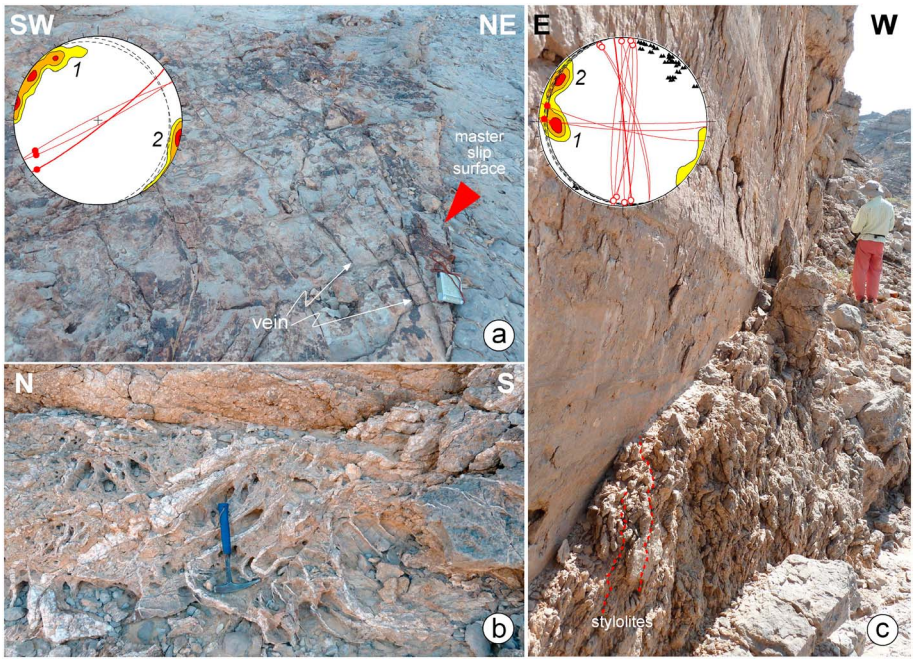

Figure 12. Examples of deformation structures in strike-slip damage zones. (a) Field locality G: plane view of a NE-SW left-lateral strike-slip fault zone developed in Natih A; note the curved trajectory of calcite veins in the southern damage zone, from fault parallel adjacent to the master slip surface, to almost N-S moving away from it. The stereonet shows structural data collected in the same fault zone: red great circles indicate the geometry and kinematics of fault zones (the trace of the master slip surface is thicker); broken great circles indicate the attitude of bedding; contouring shows the geometry of calcite veins (45 data): maximum 1 refers to fault-parallel veins while maximum 2 indicates veins at about 45° counterclockwise from the master slip surface. (b) Plane view of tightly folded calcite veins adjacent to the master slip surface of the main N-S right-lateral strike-slip fault zone exposed at field locality G in Figure 3. (c) Cross-sectional view of the corrugated N-S striking master slip surface and closely spaced NW-SE striking stylolites (foreground) in the western damage zone of the right-lateral strike-slip fault zone exposed at field site G. The master slip surface developed in Natih A, while the western damage zone developed in Natih B. The stereographic projection shows structural data collected in the same fault zone: fault geometry and kinematics are indicated by red great circles; black triangles indicate the attitude of tectonic stylolites (the trace of the master slip surface is thicker); contouring shows the attitude of calcite veins (92 data). Note that the N-S fault traces parallel the strike of bedding and of vein set 1, whereas vein set 2 lies at about 45° clockwise from the master slip surface.

2.8. Fault Cores

The internal structure of most fault cores, both in extensional and strike-slip fault zones, is quite unusual. Typically, they show impressive evidence of dilation, up to ~ 7 m, and multiple events of Group 2 and Group 3 calcite precipitation (Figure 15g), similar to the internal structure of veins in the corresponding damage zones. In this case, however, euhedral crystals frequently are pluricentimetric in size. In more detail, some fault cores still preserve layers of strongly cemented grey monogenic cataclasite associated with smoothly polished master slip surfaces (Figures 17a and 17b). In places, these cataclastic bodies are silicified. In most cases, they are bounded at one or both sides by layers of yellow-to-reddish cataclasite consisting of limestone clasts embedded into very abundant Group 2 cement made of large calcite crystals with blocky texture and frequent dark to black hydrocarbon inclusions (Figure 17c). This cataclasite generation is in turn frequently affected by further cataclasis (Figure 17d), followed by dilation and deposition of multiple generations of Group 3 layered calcite growth bands and large calcite crystals and aggregates (Figure 15g).

3. Discussion

3.1. Interpreted Evolution of the Jabal Qusaybah Anticline

The combination of structural, petrographical, and stable isotopes data allows us to propose a three-stage evolutionary pathway for the deformation pattern of the Jabal Qusaybah Anticline. For this purpose, in the conceptual sketch shown in Figure 18 vein geometry has been referred to an E-W bedding strike in order to remove possible bias created by noncylindrical folding.

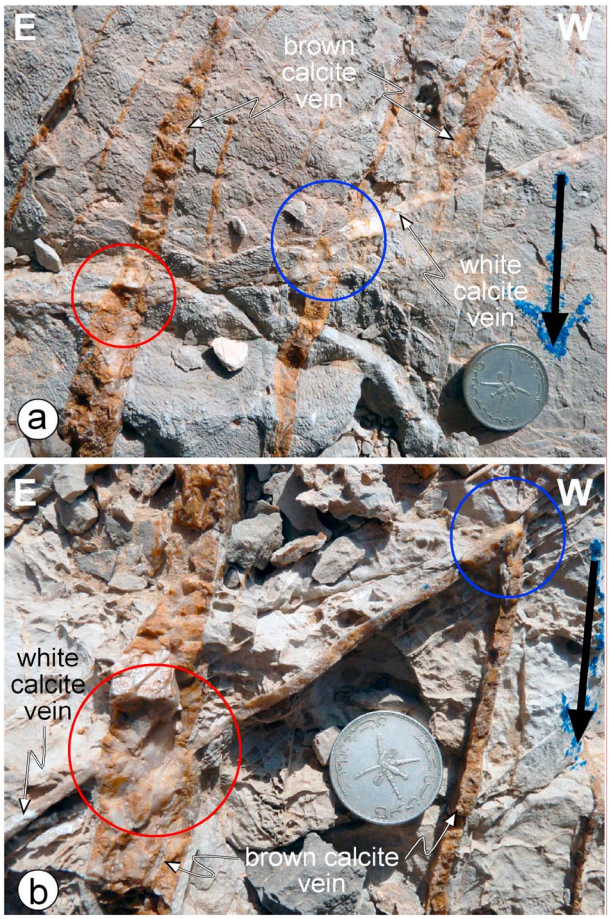

Figure 13. Plan views of different intersecting calcite vein generations along a NE-SW left-lateral strike-slip fault zone exposed at field locality D in Figure 3. (a) NE-SW striking white calcite vein offsetting a N-S brown calcite vein (blue circle) and in turn offset by another N-S brown calcite vein (red circle). (b) NE-SW striking white calcite vein offsetting a N-S brown calcite (blue circle) and in turn offset by another N-S brown calcite vein (red circle).

The first stage of the proposed model includes burial-related compaction and dissolution, which occurred concurrently with NNE-SSW and E-W veining, followed by E-W extensional faulting (Figure 18a). This inference is supported by the mutual cross-cutting relationships between Group 1 veins and bedding-parallel stylolites and by the presence of Group 1 veins in the damage zones of E-W fault zones. The presence of Group 1 NE-SW veins in the damage zones of NE-SW left-lateral strike-slip fault zones can be explained by extensional reactivation of inherited weakness zones at depth [e.g., *Filbrandt et al.*, 2006; *Al-Kindi and Richard*, 2014]. Some left-lateral NE-SW fault zones were activated at this stage, as indicated by N-S Group 1 veins in their damage zones, and likely acted as misoriented tears in extensional accommodation zones. Early right-lateral strike-slip motions along N-S fault zones occurred at this stage possibly associated with the activity of some NE-SW left-lateral fault segments.

Relative chronology indicates that NNE-SSW vertical veins were the first to form, allowing us to interpret them as developed in the foreland basin of the Oman Mountains, parallel to the trajectory of the maximum compressional axis σ_1 of the orogenic stress ellipsoid, and perpendicular to a near-horizontal σ_3, i.e., in a strike-slip stress field configuration. This is a quite common feature in many thrust-fold belts worldwide [e.g., *Ahmadhadi et al.*, 2008], possibly induced by a differential subsidence in foredeeps and related axial stretching [e.g., *Tavani et al.*, 2015]. Formation of the first generation of E-W veins started almost contemporary by cross jointing [*Bai et al.*, 2002], as indicated by the evidence that their abutting relations with N-S veins predated Group 1 calcite mineralization. Tensile failure in the southern boundary region of the Late Cretaceous foredeep [*Boote et al.*, 1990; *Ali and Watts*, 2009] induced extensional faulting during deposition of the lower Fiqa Formation in Campanian times, as indicated by the extensional growth fault zone in the foreland of the Jabal Qusaybah Anticline (Figure 6). Subsurface evidence of a Campanian extensional growth wedge in the hanging wall of the Fahud Fault to the west (Figure 1) [*Filbrandt et al.*, 2006], supports this interpretation. An E-W striking major extensional fault zone, comparable to the Fahud Fault, may have formed at this stage (Qusaybah Fault), soling down into the Ara evaporites and triggering its reactive mobilization, as tentatively interpreted in Figure 6. Due to subsequent contraction, folding, and erosion, evidence for an extensional growth wedge is not preserved in the Fiqa sediments seismically imaged in the hanging wall of the master fault. The proposed activity of the Qusaybah Fault in Campanian times rules out the possibility of Santonian positive fault inversion [*Al-Lazki et al.*, 2002].

The second stage of the proposed evolutionary model involves the reversal of the local stress field, which caused (i) the development of a weak layer-parallel shortening fabric composed by E-W bedding-perpendicular stylolites and related veins, (ii) positive inversion of the Qusaybah Fault (Figure 18b), and (iii) the reactivation of

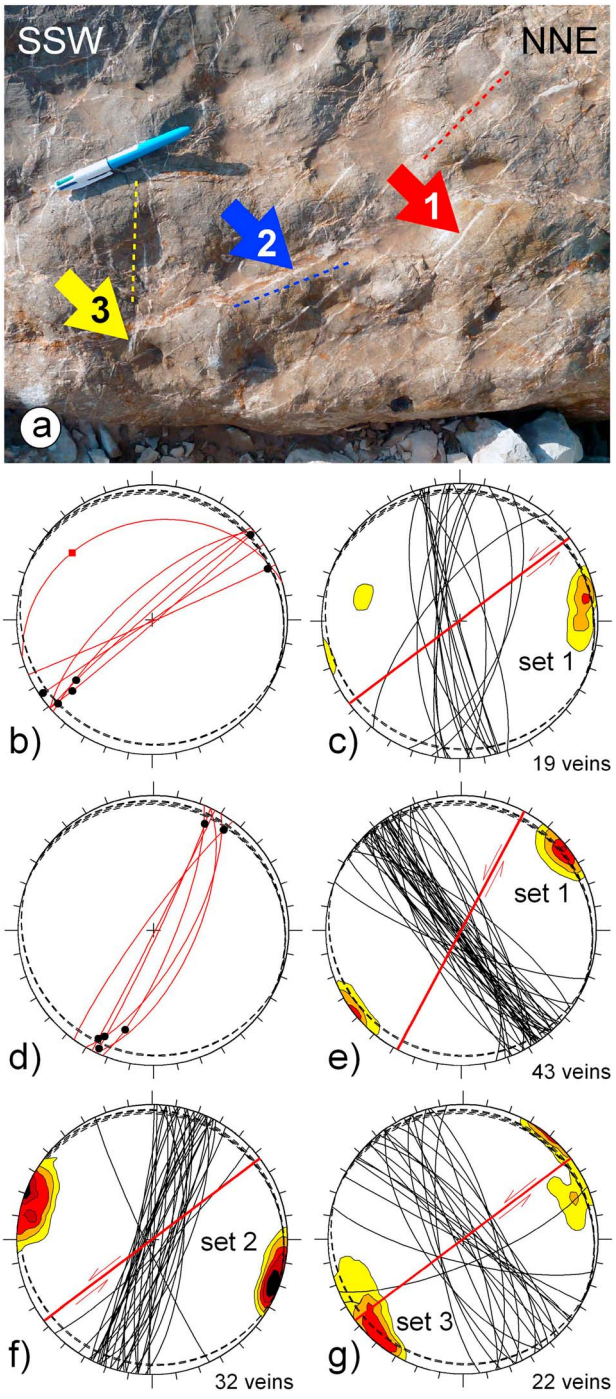

Figure 14. Vein network in the damage zone of a NE-SW left-lateral strike-slip fault zone exposed at field locality A in Figure 3. (a) Detailed plane view of a damage zone sector showing the presence of three different vein sets indicated by 1, 2, and 3. (b) Stereographic projection showing fault geometry and kinematics at site shown in Figure 14a. (c) Attitude of set 1 veins with respect to the average trend of the fault zone (shown in red). (d) Stereographic projection showing fault geometry and kinematics of an adjacent NNE-SSW splay fault. (e) Attitude of set 1 veins with respect to the average trend of the fault zone. (f) Attitude of set 2 veins with respect to the average trend of the fault zone at site shown in Figure 14a. (g) Attitude of set 3 veins with respect to the average trend of the fault zone at site shown in Figure 14a.

most of the prefolding deformation pattern. Occurrence of inversion-related early Group 2 veins (e.g., field locality G) suggests that weaker E-W extensional fault zones failed very soon after stress field reversal. This helps explaining the relative scarcity of tectonic stylolites trending parallel to the anticlinal hinge. Development of N-S extensional fault zones and related early cataclasites in between NE-SW sinistral ones likely started at this stage. The presence of similar cataclastic rocks along the latter indicates that NE-SW left-lateral strike-slip faulting triggered formation of the N-S extensional ones in transtensional horsetail arrays accommodating horizontal displacement at fault tips (Figure 18b). The evidence that E-W veins are not common in NE-SW left-lateral strike-slip damage zones, where they are frequently replaced by tectonic stylolites, indicates that folding and sinistral shearing coevally occurred. This is supported by exploitation of some NE-SW fault zones in the crestal area as fold hinge segments.

The concomitance of anticlinal folding and NE-SW left-lateral strike-slip faulting induced significant generalized dilation with progressing fold amplification, as indicated by reopening of most Group 1 veins, formation of folding-related, new approximately E-W and approximately N-S fractures with opposite abutting relations with respect to the prefolding ones, development of N-S striking extensional fault zones, dilation of fault cores, and widespread precipitation of Group 2 cements. Widespread dilation and effective hydraulic connectivity across the deformed multilayer favored migration of exotic fluids into the growing anticline, as indicated by the different isotopic signature of Group 2 calcites compared with Group 1 cements (Figure 7). Stronger prefolding E-W extensional fault zones initially resumed as tensile deformation structures by outer arc extension and where subsequently inverted (e.g., field locality E). The presence of bedding parallel Group 2 thick veins (e.g., Figure 15f) may support

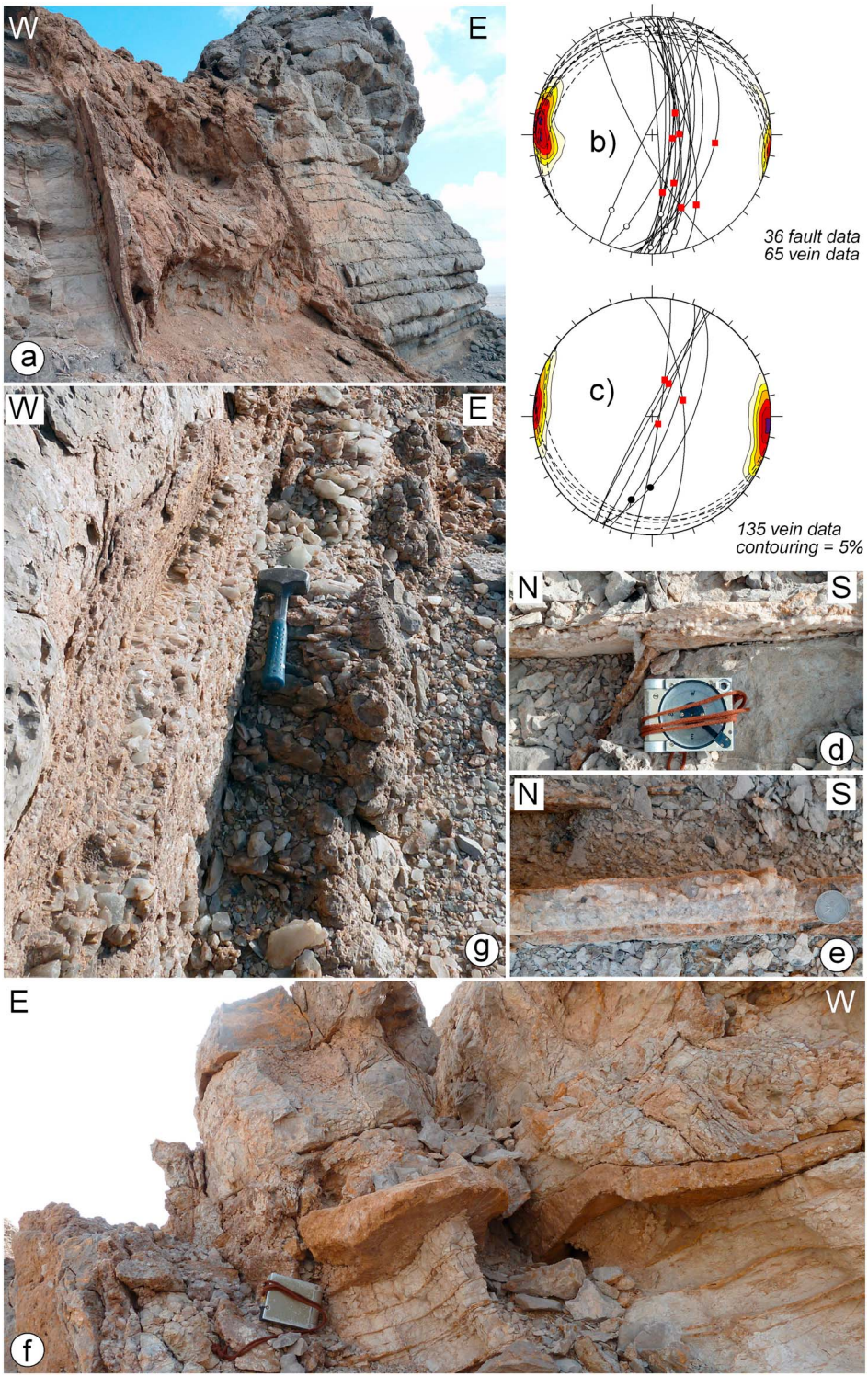

Figure 15. (a) Cross-sectional view of an extensional fault zone exposed at field locality F in Figure 3; the brownish-orange color highlights abundant iron-rich calcite precipitation. (b) Structural data collected at this field locality. (c) Structural data collected along an extensional fault zone exposed at field locality L in Figure 3. (d) Plan view of a N-S striking white calcite vein showing evidence of multiple infilling events; field locality C in Figure 3. (e) Plan view of a N-S striking brown to white calcite vein showing evidence of multiple infilling events; field locality P in Figure 3. (f) Cross-sectional view of bedding-parallel veins in the footwall damage zone of the N-S master extensional fault zone exposed at field locality P in Figure 3. (g) Plan view of a N-S extensional fault core showing evidence of multiple infilling events by alternating layers of large euhedral calcite crystals and aggregates; field locality L in Figure 3. Note that kinematic indicators on stereonets are as given in Figure 3.

Figure 16. (a) Cross-sectional view of a N-S extensional fault zone; the stereonet in the inset shows the accompanying structural data. (b) Detailed plane view of a shear lens preserved along the master extensional slip surface: closely spaced, near-vertical N-S stylolites are evident.

transient fluid overpressuring along N-S fault damage zones.

The abundance and magnitude of N-S dilational features regardless of the position within the exposed Natih Formation, indicate that this stage of fold evolution was characterized by stretching parallel to the fold axial strike associated with development of the central axial bulge that characterizes the Jabal Qusaybah anticline, with a negligible role of the mechanical stratigraphy to promote selective dilational faulting [*Ferrill and Morris*, 2003]. Axial bulging may relate with further mobilization of the Ara evaporites in the anticlinal core, which might have also acted as a strain localizator [*Callot et al*., 2012]. Indirect support to this inference is provided by the evidence that widespread occurrence of severely dilated fault zones and related infill by very large calcite crystals and aggregates has been also described in Jabal Madar anticline, ~ 110 km to the east (Figure 1), where a salt diapir is well documented [e.g., *Immenhauser et al*., 2007; *Claringbould et al*., 2013]. The isotopic signatures of these crystals in Jabal Madar [*Immenhauser et al*., 2007] and for one of the calcite crystal populations in Jabal Qusaybah are very similar.

Evidence for positive fault inversion is common in the foreland of the Oman Mountains, mainly by Cenozoic reactivation of E-W to WNW-ESE extensional fault zones formed in Late Cretaceous times during the obduction of oceanic lithosphere onto Mesozoic platform carbonates of the continental margin in North Oman [*Robertson*, 1987; *Loosveld et al*., 1996; *Filbrandt et al*., 2006; *Al-Kindi and Richard*, 2014; *Cooper et al*., 2014]. Ongoing plate convergence eventually led to the formation of the Oman Mountains foreland thrust-fold belt, mainly in Oligocene to Pliocene times, including shortening in the Salakh Arch [*Searle*, 1985; *Mount et al*., 1998; *Poupeau et al*., 1998; *Al-Lazki et al*., 2002; *Filbrandt et al*., 2006; *Fournier et al*., 2006; *Agard et al*., 2010]. The main positive inversion pulse of the Jabal Qusaybah extensional fault system can be constrained by the burial history of the Natih Formation and its overburden in the foreland basin, which shows a reversal from subsidence to uplift in Miocene times [*Terken*, 1999]. Miocene positive inversion of extensional fault zones affecting the Arabian platform has been proposed from a regional geological and geophysical study across the Northern Emirates [*Tarapoanca et al*., 2010].

The third stage of the proposed evolutionary pathway includes fold tightening and development of a footwall splay thrust, final amplification of the axial bulge during progressive exhumation of the anticline, and prosecution of N-S extensional faulting in an overall dilational environment (Figure 18c). This inference is supported by the widespread reopening of the preexisting deformation pattern and abundant precipitation of Group 3 calcite cements (Figure 7a). Some activity of the NE-SW left-lateral strike-slip fault zones still

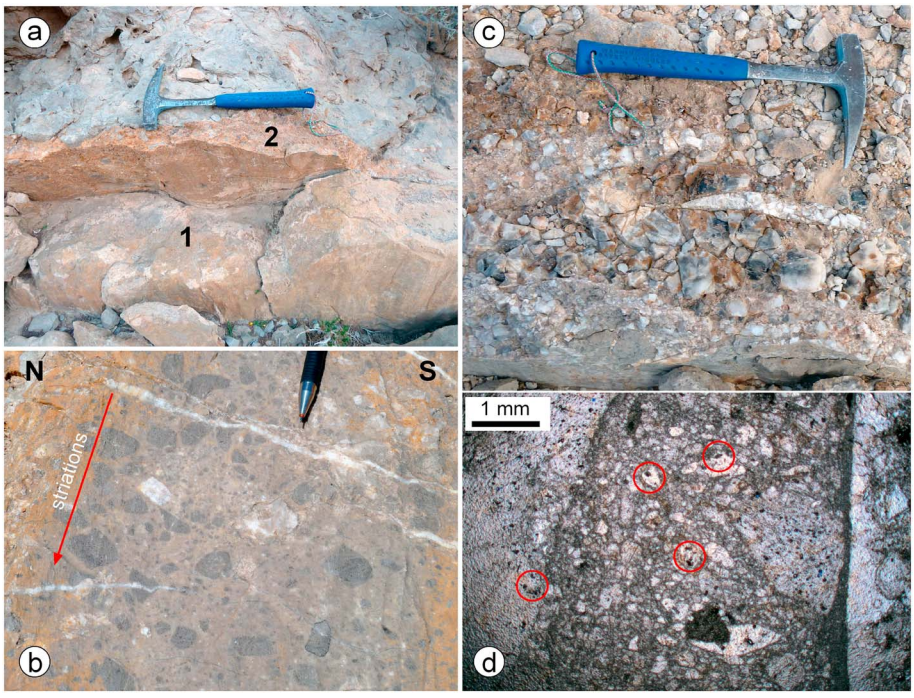

Figure 17. Main features of fault cores. (a) Layer of strongly cemented monogenic cataclasite (1, in the foreground) that underwent further dilation on one side and infilling by iron-rich calcite (2); field locality C in Figure 3. (b) Detail of a polished master slip surface in strongly cemented monogenic cataclasite: the presence of white calcite veins cutting through the cataclasite and striking perpendicular to abrasion-related striations indicate fault activity after cataclasite cementation; field locality P in Figure 3. (c) Detailed plane view of calcite crystals and aggregates deposited in the hanging wall side of a dilated master slip surface at field locality C in Figure 3; several events of cracking and sealing by different calcite generations are evident. (d) Photomicrograph of a calcite vein with hydrocarbon inclusions (some of them are highlighted by red circles), affected by further cataclasis; same fault zone as in Figure 17c.

occurred at this time, despite being strongly subordinate to late stage longitudinal stretching. We speculate that the final evolution of the Jabal Qusaybah anticline may have occurred in Pliocene times or even later, because of the excellent preservation of many fault-related morphological features.

3.2. Speculations on the Cause for Concomitant NE-SW Left-Lateral Strike-Slip Faulting and Folding in the Jabal Quasaybah Anticline and Salakh Arc

The presence of widespread NE-SW left-lateral strike-slip faulting associated with E-W fold growth is not a typical feature of positive fault inversion and cylindrical folding in general. Attempts to explain NE-SW strike-slip and N-S extensional faulting as a kinematic mechanism triggered by progressive arching in a foreland salient [*Hanna and Smewing*, 1996] fail to successfully reproduce actual shear senses. In fact, southward amplification and extrusion of the Salakh Arch would have been mainly accommodated by NE-SW right-lateral rather than left-lateral strike-slip faulting in Jabal Qusaybah. Left-lateral strike-slip reactivation of the inherited E-W extensional Qusaybah Fault in a transpressional basin inversion scenario [e.g., *Mattioni et al*., 2007] cannot be neglected and is expected to induce NE-SW to ENE-WSW synthetic shearing near the surface, analogously to what has been described for the Fahud Fault [*Al-Kindi and Richard*, 2014]. However, the E-W axial trend of the Jabal Qusaybah anticline, near-perpendicular to the regional maximum compressional direction, does not favor significant left-lateral shearing on the inherited extensional fault zone at depth. This is supported by the lack of any evidence of E-W left-lateral strike-slip fault zones in the visited outcrops.

Involvement of the Ara evaporites and the presence of a variable thickness overburden may provide the appropriate additional factor that can help explaining the peculiar fault-fold kinematics described in the Jabal Qusaybah anticline. Despite not properly scaled for the specific Oman case, sandbox analog modeling of thrust wedge development above a salt layer characterized by very gentle, foredeep-parallel tapering of the overburden (Figure 18d) showed that the combination of tectonic and gravitational forces triggered

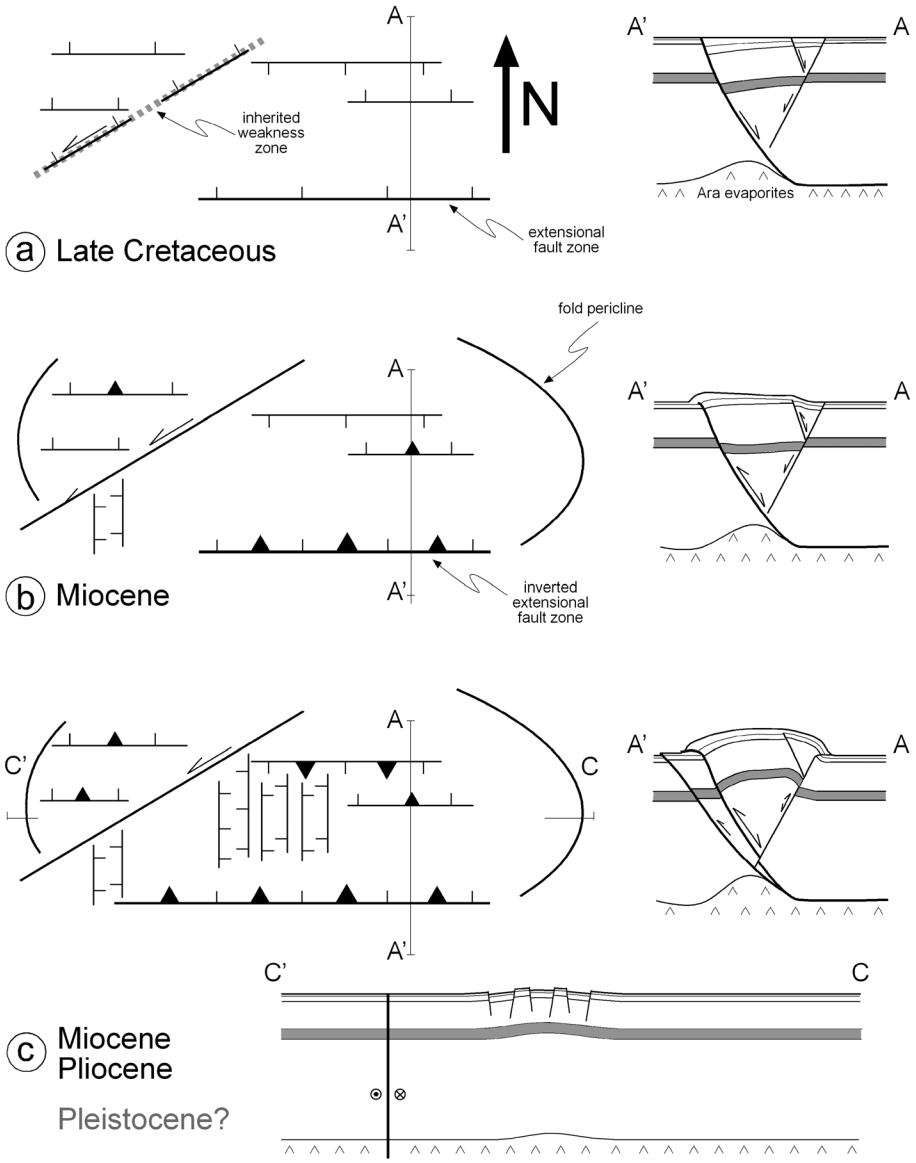

Figure 18. (a–c) Conceptual cartoon showing the proposed evolution of faulting and folding in (left) map view and (right) cross sections of the Jabal Qusaybah anticline. Not to scale; see text for details.

development of a complex fault pattern where partitioned transpression and transtension favored oblique extrusion of the frontal thrust sheet along strike-slip fault zones striking at about 45° from the fold axial trend [*Storti et al.*, 2007] (Figure 18d). Application of this scenario to the toe region of the Oman Mountains thrust wedge implies (i) a thicker sedimentary or tectonic overburden of the Ara evaporites in the eastern part of the Salakh Arc area and (ii) occurrence of NE-SW left-lateral strike-slip fault zones all across the Salakh Arc and not limited to the Jabal Qusaybah anticline. Condition (i) may have occurred because crustal accretion from both the NNE (Semail Ophiolite in the Oman Mountains) and ESE (Masirah Ophiolite in East Oman) might have induced foredeep preferential subsidence toward the east [*Terken*, 1999]. Condition (ii) is satisfied because NE-SW trending fractures, including left-lateral strike-slip fault zones, are described in other anticlines of the Salakh Arch [e.g., *Bazalgette*, 2004; *De Keijzer et al.*, 2007].

4. Conclusions

We performed a structural and petrographical-geochemical study of deformation structures exposed in the Jabal Qusaybah anticline, at the western termination of the Salakh Arch, a major salient at the toe of the

Oman Mountains thrust wedge. Field and laboratory data have been integrated with the analysis of a reflection seismic profile cutting through the western periclinal termination of the fold. The results of our work can be summarized in the following points.

1. The deformation pattern characterizing the E-W trending Jabal Qusaybah anticline includes NE-SW left-lateral strike-slip and N-S extensional fault zones. Petrographical features, $\delta^{13}C$ and $\delta^{18}O$ stable isotope signatures of differentiated calcite vein infills, and the geometric, kinematic, and overprinting relationships of calcite veins indicate that folding and faulting occurred coevally during the growth of the anticline.
2. In the central sector of the anticlinal crest, the fold axis has a gentle along-strike bump. There, N-S striking extensional fault zones subperpendicular to the fold axis are abundant and abut the NE-SW left-lateral strike-slip fault zones. Both strike-slip and extensional fault zones show widespread evidence for impressive dilation in the form of infilling by large calcite crystals and aggregates. This is particularly outstanding along the N-S extensional fault zones where the magnitude of fault core dilation frequently exceeds 1 m.
3. A plausible kinematic pathway that could explain the coexistence of such unusual noncylindrical synfolding deformation pattern in the Jabal Qusaybah anticline involves mobilization of the underlying Ara evaporites under a foredeep-parallel tapering overburden wedge of sedimentary and/or tectonic origin. This geometry would add a component of southeastward extrusion to the evolution of the Salakh Arch, thus helping to trigger NE-SW left-lateral strike-slip faulting, and would have favored longitudinal axial bulging of the anticline accompanied by generalized dilation in the central region of the crest. Some possible left-lateral shearing along the inherited E-W Qusaybah extensional fault system at depth cannot be ruled out but is not supported by the available field data.

Finally, this work illustrates how complex deformation patterns can be in fault-related anticlines that develop near or within curved segments of major thrusts. Conventional templates for folding-related fracturing do not predict the occurrence of either fault-perpendicular extensional or obliquely striking transcurrent fault systems, which can strongly impact vertical hydraulic connectivity and fluid flow. Similar atypical fault and fold patterns could be expected in structures at the toe of thrust wedges and so should be incorporated into conceptual models of those structures.

Acknowledgments

This work is part of a joint research project between Parma and KU Leuven universities funded by Shell Global Solutions. We are grateful to Shell for releasing this material for publication. We are also grateful to L. Barchi and A. Comelli for support with SEM analyses and thin-section preparation, respectively. Also, H. Nijs is acknowledged for thin-section preparation. We warmly thank F. Mondino (formerly at Shell) for the enthusiastic support she gave to the early stages of this project. The source data of the diagrams presented in this article are proprietary of Shell Global Solutions and, for confidentiality agreements, cannot be released for free download. The manuscript benefited from discussions with L. Bazalgette, A. Koopman, and P. Richard and from the constructive criticism and suggestions of two anonymous reviewers and the Associate Editor. We acknowledge editorial handling by C. Faccenna. Stereographic projections were made by using the Daisy3 software [*Salvini*, 2014].

References

Agard, P., M. P. Searle, G. I. Alsop, and B. Dubacq (2010), Crustal stacking and expulsion tectonics during continental subduction: P-T deformation constraints from Oman, *Tectonics*, *29*, TC5018, doi:10.1029/2010TC002669.

Ahmadhadi, F., J. M. Daniel, M. Azzizadeh, and O. Lacombe (2008), Evidence for pre-folding vein development in the Oligo-Miocene Asmari Formation in the Central Zagros Fold Belt, Iran, *Tectonics*, *27*, TC1016, doi:10.1029/2006TC001978.

Ali, M. Y., and A. B. Watts (2009), Subsidence history, gravity anomalies and flexure of the United Arab Emirates (UAE) foreland basin, *GeoArabia*, *14*, 17–44.

Al-Kindi, M. H. (2006), Structural evolution and fracture pattern of Salakh Arch, PhD thesis, Univ. of Leeds.

Al-Kindi, M. H., and P. D. Richard (2014), The main structural styles of the hydrocarbon reservoirs in Oman, *Geol. Soc. London Spec. Publ.*, *392*, 409–445, doi:10.1144/SP392.20.

Al-Lazki, A., D. Seber, E. Sandvol, and M. Barazangi (2002), A crustal transect across the Oman Mountains on the eastern margin of Arabia, *GeoArabia*, *7*, 47–78.

Amrouch, K., O. Lacombe, N. Bellahsen, J.-M. Daniel, and J.-P. Callot (2010), Stress and strain patterns, kinematics and deformation mechanisms in a basement-cored anticline: Sheep Mountain Anticline, Wyoming, *Tectonics*, *29*, TC1005, doi:10.1029/2009TC002525.

Anastasio, D. J., and J. E. Holl (2001), Transverse fold evolution in the External Sierra, southern Pyrenees, Spain, *J. Struct. Geol.*, *23*, 379–392.

Bai, T., L. Maertens, M. R. Gross, and A. Aydin (2002), Orthogonal cross joints: Do they imply a regional stress rotation?, *Tectonophysics*, *576*, 20–45.

Barbier, M., Y. Hamon, J.-P. Callot, M. Floquet, and J.-M. Daniel (2012a), Sedimentary and diagenetic controls on the multiscale fracturing pattern of a carbonate reservoir: The Madison Formation (Sheep Mountain, Wyoming, USA), *Mar. Pet. Geol.*, *29*, 50–67.

Barbier, M., R. Lepretre, J.-P. Callot, M. Gasparrini, J.-M. Daniel, Y. Hamon, O. Lacombe, and M. Floquet (2012b), Impact of fracture stratigraphy on the paleo-hydrogeology of the Madison Limestone in two basement-involved folds in the Bighorn basin, (Wyoming, USA), *Tectonophysics*, *576-577*, 116–132.

Barrier, L., T. Nalpas, D. Gapais, J. N. Proust, A. Casas, and S. Bourquin (2002), Influence of syntectonic sedimentation on thrust geometry. Field examples from the Iberian Chain (Spain) and analogue modelling, *Sediment. Geol.*, *146*, 91–104.

Bazalgette, L. (2004), Relations plissement/fracturation multi-échelle dans les multicouches sédimentaires du domaine élastique fragile, PhD thesis, 252 pp., Université de Montpellier II, 17 Dec.

Beaudoin, N., R. Lepretre, N. Bellahsen, O. Lacombe, K. Amrouch, J.-P. Callot, L. Emmanuel, and J.-M. Daniel (2012), Structural and microstructural evolution of the Rattlesnake Mountain Anticline (Wyoming, USA): New insights into the Sevier and Laramide orogenic stress build-up in the Bighorn Basin, *Tectonophysics*, *576-577*, 20–45.

Beaudoin, N., O. Lacombe, N. Bellahsen, and L. Emmanuel (2013), Contribution of studies of sub-seismic fracture populations to paleo-hydrological reconstructions (Bighorn Basin, USA), *Procedia Earth Planet. Sci.*, *7*, 57–60.

Bellahsen, N., P. E. Fiore, and D. D. Pollard (2006), From spatial variation of fracture patterns to fold kinematics: A geomechanical approach (2006), *Geophys. Res. Lett.*, *33*, L02301, doi:10.1029/2005GL024189.

Boote, D. R. D., D. Mou, and R. I. Waite (1990), Structural evolution of the Suneinah Foreland, Central Oman Mountains, *Geol. Soc. London Spec. Publ.*, *49*, 397–418, doi:10.1144/GSL.SP.1992.049.01.25.
Burkhard, M. (1993), Calcite twins, their geometry, appearance and significance as stress-strain markers and indicators of tectonic regime: A review, *J. Struct. Geol.*, *15*, 351–368.
Callot, J.-P., L. Breesch, N. Guilhaumou, F. Roure, R. Swennen, and N. Vilasi (2010), Paleo-fluids characterisation and fluid flow modelling along a regional transect in Northern United Arab Emirates (UAE), *Arabian J. Geosci.*, *3*, 413–437.
Callot, J.-P., V. Trocmé, J. Letouzey, E. Albouyi, S. Jahani, and S. Sherkati (2012), Pre-existing salt structures and the folding of the Zagros Mountain, *Geol. Soc. London Spec. Publ.*, *363*, 545–561.
Chester, J. S. (2003), Mechanical stratigraphy and fault-fold interaction, Absaroka thrust sheet, Salt River Range, Wyoming, *J. Struct. Geol.*, *25*, 1171–1192.
Chester, J. S., J. M. Logan, and J. H. Spang (1991), Influence of layering and boundary conditions on fault-bend and fault-propagation folding, *Geol. Soc. Am. Bull.*, *103*, 1059–1072, doi:10.1130/0016-7606(1991)103.
Claringbould, J. S., B. B. Hyden, J. F. Sarg, and B. D. Trudgill (2013), Structural evolution of a salt-cored, domed, reactivated fault complex, Jebel Madar, Oman, *J. Struct. Geol.*, *51*, 118–131.
Cooper, D. J. W., M. Y. Ali, M. P. Searle, C. Park, T. Wells, P. O. Box, A. Dhabi, and U. A. Emirates (2014), Structure of the northern Oman Mountains from the Semail Ophiolite to the Foreland Basin, in *Tectonic Evolution of the Oman Mountains*, edited by H. R. Rollinson et al., *Geol. Soc. London Spec. Publ.*, *392*, 129–153.
Cooper, M. (1992), The analysis of fracture systems in subsurface thrust structures from the foothills of the Canadian Rockies, in *Thrust Tectonics*, edited by K. R. McClay, pp. 391–405, Chapman and Hall, London.
Corbett, K., M. Friedman, and M. Spang (1987), Fracture development and mechanical stratigraphy of Austin Chalk, Texas, *Am. Assoc. Pet. Geol. Bull.*, *71*, 17–28.
Couzens, B. A., and D. W. Wiltschko (1996), The control of mechanical stratigraphy on the formation of triangle zones, *Bull. Can. Pet. Geol.*, *44*, 165–179.
De Keijzer, M., H. Hillgartner, S. Al Dhahab, and K. Rawnsley (2007), A surface-subsurface study of reservoir-scale fracture heterogeneities in Cretaceous carbonates, North Oman, *Geol. Soc. London Spec. Publ.*, *270*, 227–244, doi:10.1144/GSL.SP.2007.270.01.15.
Di Naccio, D., P. Boncio, S. Cirilli, F. Casaglia, E. Morettini, G. Lavecchia, and F. Brozzetti (2005), Role of mechanical stratigraphy on fracture development in carbonate reservoirs: Insights from outcropping shallow water carbonates in the Umbria–Marche Apennines, Italy, *J. Volcanol. Geotherm. Res.*, *148*(1), 98–115.
Dickson, J. A. D. (1966), Carbonate identification and genesis as revealed by staining, *J. Sediment. Petrol.*, *36*, 491–505.
Erslev, E. A., and K. R. Mayborn (1997), Multiple geometries and model of fault propagation folding in the Canadian thrust belt, *J. Struct. Geol.*, *19*, 321–335.
Evans, M. A., and M. P. Fischer (2012), On the distribution of fluids in folds: A review of controlling factors and processes (2012), *J. Struct. Geol.*, *44*, 2–24.
Ferrill, D. A., and A. P. Morris (2003), Dilational normal faults, *J. Struct. Geol.*, *25*, 183–196, doi:10.1016/S0191-8141(02)00029-9.
Filbrandt, J. B., S. Al-Dhahab, A. Al-Habsy, K. Harris, J. Keating, S. Al-Mahruqi, S. I. Ozkaya, P. D. Richard, and T. Robertson (2006), Kinematic interpretation and structural evolution of North Oman, Block 6, since the Late Cretaceous and implications for timing of hydrocarbon migration into Cretaceous reservoirs, *GeoArabia*, *11*, 97–140.
Fischer, M. P., and P. B. Jackson (1999), Stratigraphic controls on deformation patterns in fault-related folds: A detachment fold example from the Sierra Madre Oriental, northeast Mexico, *J. Struct. Geol.*, *21*, 613–633.
Fischer, M. P., N. B. Woodward, and M. M. Mitchell (1992), The kinematics of break-thrust folds, *J. Struct. Geol.*, *14*, 451–460.
Fournier, M., C. Lepvrier, P. Razin, and L. Jolivet (2006), Late Cretaceous to Paleogene Post-obduction extension and subsequent Neogene compression in Oman Mountains, *GeoArabia*, *11*, 17–40.
Gross, M. R. (1995), Fracture partitioning: Failure mode as a function of lithology in the Monterey Formation of coastal California, *Geol. Soc. Am. Bull.*, *107*, 779–792.
Guiton, M. L. E., W. Sassi, Y. M. Leroy, and B. D. M. Gauthier (2003), Mechanical constraints on the chronology of fracture activation in folded Devonian sandstone of the western Moroccan Anti-Atlas, *J. Struct. Geol.*, *25*, 1317–1330.
Hancock, P. L. (1985), Brittle microtectonics: Principles and practice, *J. Struct. Geol.*, *7*, 437–457.
Hanna, S. S. (1990), The Alpine deformation of the Central Oman Mountains, *Geol. Soc. London Spec. Publ.*, *49*, 341–359, doi:10.1144/GSL.SP.1992.049.01.21.
Hanna, S. S., and J. D. Smewing (1996), *The Stratigraphy and Structure of the Madamar-Salakh-Qusaybah Range and Natih-Fahud Area in the Oman Mountains*, *J. Sci. Technol.*, vol. 1, pp. 1–19, Sultan Qaboos Univ., Oman.
Homewood, P., P. Razin, C. Grelaud, H. Droste, V. Vahrenkamp, M. Mettraux, and J. Mattner (2008), Outcrop sedimentology of the Natih Formation, northern Oman: A field guide to selected outcrops in the Adam Foothills and Al Jabal al Akhdar areas, *GeoArabia*, *13*, 39–120.
Immenhauser, A., A. Creusen, M. Esteban, and H. B. Vonhof (2000), Recognition and interpretation of polygenic discontinuity surfaces in the Middle Cretaceous Shu'aiba, Nahr Umr, and Natih Formations of Northern Oman, *GeoArabia*, *5*, 299–322.
Immenhauser, A., Y. V. Dublyansky, K. Verwer, D. Fleitman, and S. E. Pashenko (2007), Textural, elemental, and isotopic characteristics of Pleistocene phreatic cave deposits (Jabal Madar, Oman), *J. Sediment. Res.*, *77*, 68–88.
Jahani, S., J.-P. Callot, J. Letouzey, and D. Frizon de Lamotte (2009), The eastern termination of the Zagros Fold-and-Thrust Belt, Iran: Structures, evolution, and relationships between salt plugs, folding, and faulting, *Tectonics*, *28*, TC6004, doi:10.1029/2008TC002418.
Jamison, W. R. (1992), Stress controls on fold thrust style, in *Thrust Tectonics*, edited by K. R. Mcclay, pp. 155–164, Chapman & Hall, London.
Lemiszki, P. J., J. D. Landes, and R. D. Hatcher (1994), Controls on hinge-parallel extension fracturing in single-layer tangential-longitudinal strain folds, *J. Geophys. Res.*, *99*, 22,027–22,041, doi:10.1029/94JB01853.
Loosveld, R. J. H., A. Bell, and J. J. M. Terken (1996), The tectonic evolution of interior Oman, *GeoArabia*, *1*, 28–51.
Macedo, J., and S. Marshak (1999), Controls on the geometry of fold-thrust belt salients, *Geol. Soc. Am. Bull.*, *111*, 1808–1822.
Marshak, S. (1988), Kinematics of orocline and arc formation in thin-skinned orogens, *Tectonics*, *7*, 73–86, doi:10.1029/TC007i001p00073.
Mattioni, L., W. Sassi, and J.-P. Callot (2007), Analogue models of basin inversion by transpression: Role of structural heterogeneity, *Geol. Soc. London Spec. Publ.*, *272*, 397–417.
Mount, V. S., R. I. S. Crawford, and S. C. Bergman (1998), Regional structural style of the central and southern Oman Mountains, Jebel Akhdar, Saih Hatat, and the northern Ghaba Basin, *GeoArabia*, *3*, 475–490.
Muñoz, J.-A., E. Beamud, O. Fernandez, P. Arbues, J. Dinares-Turell, and J. Poblet (2013), The Ainsa Fold and thrust oblique zone of the central Pyrenees: Kinematics of a curved contractional system from paleomagnetic and structural data, *Tectonics*, *32*, 1142–1175, doi:10.1002/tect.20070.
Poupeau, G., O. Saddiqi, A. Michard, B. Goffe, and R. Oberhansli (1998), Late thermal evolution of the Oman Mountains subophiolitic windows: Apatite fission-track thermochronology, *Geology*, *26*, 1139–1142, doi:10.1130/0091-7613(1998)026.

Protzman, G. M., and G. Mitra (1990), Strain fabric associated with the Meade thrust sheet: Implications for cross-section balancing, *J. Struct. Geol.*, *12*, 403–417.
Richard, P., B. Mocquet, and P. R. Cobbold (1991), Experiments on simultaneous faulting and folding above a basement wrench fault, *Tectonophysics*, *188*, 133–141.
Robertson, A. (1987), The transition from a passive margin to an Upper Cretaceous foreland basin related to ophiolite emplacement in the Oman Mountains, *Geol. Soc. Am. Bull.*, *99*, 633–653.
Roure, F., R. Swennen, F. Schneider, J. L. Faure, H. Ferket, N. Guilhaumou, K. Osadetz, P. Robion, and V. Vandeginste (2005), Incidence and importance of tectonics and natural fluid migration on reservoir evolution in foreland fold-and-thrust belts, *Oil Gas Sci. Technol.*, *60*, 67–106.
Salvini, F. (2014), Daisy3, the Structural Data Integrated System Analyzer, *Software*, version 4.95.08. [Available at http://host.uniroma3.it/progetti/fralab.]
Sassi, W., M. L. E. Guiton, Y. M. Leroy, J.-M. Daniel, and J.-P. Callot (2012), Constraints on bed scale fracture chronology with a FEM mechanical model of folding: The case of Split Mountain (Utah, USA), *Tectonophysics*, *576-577*, 197–215.
Searle, M. P. (1985), Sequence of thrusting and origin of culminations in the northern and central Oman Mountains, *J. Struct. Geol.*, *7*, 129–143.
Stearns, D. W. (1968), Certain aspects of fracture in naturally deformed rocks, in *National Science Foundation Advanced Science Seminar in Rock Mechanics, Spec. Rep.*, edited by R. E. Rieker, pp. 97–118, Air Force Cambridge Research Laboratories, Bedford, Mass.
Storti, F., and F. Salvini (1996), Progressive rollover fault-propagation folding: A possible kinematic mechanism to generate regional-scale recumbent folds in shallow foreland belts, *Am. Assoc. Pet. Geol. Bull.*, *80*, 174–193.
Storti, F., R. Soto Marín, F. Rossetti, and A. M. Casas Sainz (2007), Evolution of experimental thrust wedges accreted from along-strike tapered, silicone-floored multilayers, *J. Geol. Soc. London*, *164*, 73–85.
Suppe, J. (1983), Geometry and kinematics of fault-bend folding, *Am. J. Sci.*, *283*, 684–721.
Swennen, R., H. Ferket, L. Benchilla, F. Roure, and R. Ellam (2003), Fluid flow and diagenesis in carbonate dominated Foreland Fold and Thrust Belts: Petrographic inferences from field studies of late-diagenetic fabrics from Albania, Belgium, Canada, Mexico and Pakistan, *J. Geochem. Explor.*, *78*, 481–485.
Tarapoanca, M., P. Andriessen, K. Broto, L. Chérel, N. Ellouz-Zimmermann, J.-L. Faure, A. Jardin, C. Naville, and F. Roure (2010), Forward kinematic modelling of a regional transect in the Northern Emirates using geological and apatite fission track age constraints on paleo-burial history, *Arabian J. Geosci.*, *3*, 395–411.
Tavani, S., F. Storti, O. Fernández, J. A. Muñoz, and F. Salvini (2006), 3-D deformation pattern analysis and evolution of the Anisclo anticline, southern Pyrenees, *J. Struct. Geol.*, *28*, 695–712.
Tavani, S., F. Storti, F. Salvini, and C. Toscano (2008), Stratigraphic versus structural control on the deformation pattern associated with the evolution of the Mt. Catria anticline, Italy, *J. Struct. Geol.*, *30*, 664–681.
Tavani, S., F. Storti, O. Lacombe, A. Corradetti, J. A. Muñoz, and S. Mazzoli (2015), A review of deformation pattern templates in foreland basin systems and fold-and-thrust-belts: Implications for the state of stress in the frontal regions of thrust wedges, *Earth Sci. Rev.*, *141*, 82–104.
Terken, J. M. J. (1999), The Natih Petroleum System of North Oman, *GeoArabia*, *4*, 157–180.
Woodward, N. B., and E. Rutherford Jr. (1989), Structural lithic units in external orogenic zones, *Tectonophysics*, *158*, 247–258.